Multi-RIS-aided Wireless Systems: Statistical Characterization and Performance Analysis

Tri Nhu Do, *Member, IEEE,* Georges Kaddoum, *Senior Member, IEEE,* Thanh Luan Nguyen, Daniel Benevides da Costa, *Senior Member, IEEE,* and Zygmunt J. Haas, *Fellow, IEEE*

***Abstract*—In this paper, we study the statistical characterization and modeling of distributed multi-reconfigurable intelligent surface (RIS)-aided wireless systems. Specifically, we consider a practical system model where the RISs with different geometric sizes are distributively deployed, and wireless channels associated to different RISs are assumed to be independent but not identically distributed (i.n.i.d.). We propose two purpose-oriented multi-RIS-aided schemes, namely, the exhaustive RIS-aided (ERA) and opportunistic RIS-aided (ORA) schemes. In the ERA scheme, all RISs participate in assisting the communication of a pair of transceivers, whereas in the ORA scheme, only the most appropriate RIS participates and the remaining RISs are utilized for other purposes. A mathematical framework, which relies on the method of moments, is proposed to statistically characterize the end-to-end (e2e) channels of these schemes. It is shown that either a Gamma distribution or a LogNormal distribution can be used to approximate the distribution of the magnitude of the e2e channel coefficients in both schemes. With these findings, we evaluate the performance of the two schemes in terms of outage probability (OP) and ergodic capacity (EC), where tight approximate closed-form expressions for the OP and EC are derived. Representative results show that the ERA scheme outperforms the ORA scheme in terms of OP and EC. Nevertheless, the ORA scheme gives a better energy efficiency (EE) in a specific range of the target spectral efficiency (SE). In addition, under i.n.i.d. fading channels, the reflecting element setting and location setting of RISs have a significant impact on the overall system performance of both the ERA or ORA schemes. A centralized large-RIS-aided scheme might achieve higher EC than the distributed ERA scheme when the large-RIS is located near a transmitter or a receiver, and vise-versa.**

***Index Terms*—Reconfigurable intelligent surface, statistical characterization, Gamma distribution, LogNormal distribution, method of moments, ergodic capacity, outage probability.**

I. Introduction

Reconfigurable intelligent surfaces (RISs) have recently been prospected as one of the key technologies to achieve smart radio environment (SRE) for the sixth generation (6G) of wireless communications [1]. Specifically, in order to create a truly SRE, one of the key requirements is to make the radio medium controllable [1]. To this end, RISs, also known as intelligent reflecting surfaces (IRSs) [2] or software-defined metasurfaces (SDMs) [3], have been developed. In particular, a RIS consists of nearly-passive reflecting elements, which are programmable and controllable via a RIS controller, allowing it to reflect and steer impinging signals toward desired directions. In order to realize this goal, the phase-shifts of the reflecting elements are adjusted, such that the directionality of the beam of scattered signals can be controlled. With this phase-tuning capability, *coherent signal combining* of reflecting signals from different elements of different RISs can be properly implemented such that the multi-path received signals are constructively added at the receiver side [3]–[5].

Single-RIS-aided systems have been extensively studied in the literature [6]–[13]. In [6], the authors presented an analytical representation of the ideal phase-shift configuration that maximizes the signal-to-noise ratio (SNR) of the synthesized received signal. In [7], considering a large intelligent surface (LIS)-aided single-input single-output (SISO) system without the direct link, the authors showed that the magnitude of the end-to-end (e2e) channel coefficient under Rayleigh fading can approximately follow a Gamma distribution. In [8], similar to [7], considering a large reflecting surface (LRS)-aided SISO system under Rayleigh fading, the authors showed that the magnitude of the e2e channel coefficient approximately follows a Nakagami distribution. In [9], considering a similar system setting as in [7] and [8], the authors derived approximate closed-form expressions for the probability density function (PDF) and cumulative distribution function (CDF) of the magnitude of the e2e channel coefficient. In [10], considering a single-RIS-aided system under Nakagami-m fading, the authors derived approximate closed-form expressions for the PDF and CDF of the e2e SNR. In [11], considering a single-RIS-aided system under Rician fading, the authors relied on the central limit theorem (CLT) to show that the magnitude of the e2e channel coefficient (without the direct channel coefficient) approximately follows a Gaussian distribution. The aforementioned works made a typical assumption that channels associated to different reflecting elements of the same RIS are independent and identically distributed (i.i.d.). In [12], the authors showed that i.i.d. Rayleigh fading does not physically occur when using a single RIS in an isotropic scattering environment. In [13], considering a single-RIS-assisted system over spatially correlated Rayleigh fading channels, the authors showed that the distribution of the e2e SNR can be approximated by a Gamma distribution.

In this work, we focus on a more general system setup and

T. N. Do and G. Kaddoum are with the Department of Electrical Engineering, ÉTS, University of Québec, Montreal, QC, Canada (emails: tri-nhu.do.1@ens.etsmtl.ca, georges.kaddoum@etsmtl.ca).

T. L. Nguyen is with the Faculty of Electronics Technology, Industrial University of HCMC, HCMC 700000, Vietnam.

D. B. da Costa is with the Future Technology Research Center, National Yunlin University of Science and Technology, Douliou, Yunlin 64002, Taiwan, R.O.C, and with the Department of Computer Engineering, Federal University of Ceará (UFC), Sobral 62010-560, Brazil (e-mail: danielbcosta@ieee.org).

Z. J. Haas is with the Department of Computer Science, University of Texas at Dallas, Richardson, TX 75080 USA, and also with the School of Electrical and Computer Engineering, Cornell University, Ithaca, NY 14853 USA (e-mail: zhaas@cornell.edu).

consider multi-RIS-aided systems. Next, we discuss some recent papers which assume such a system configuration. In [4], considering a multi-RIS-aided SISO system with direct link under i.i.d. Nagakami-m fading channels, the authors relied on the CLT to show that the magnitude of the e2e channel coefficient can approximately follow a Gaussian distribution. In [14], considering a LIS-aided system under Rician fading, where the LIS consists of RIS units and each RIS unit has a large number of reflecting elements, the authors relied on the law of large numbers and the CLT to approximate the distributions of random variables (RVs), which are functions of the squared magnitude of the channel coefficient, by Gaussian distributions. In [15], the authors considered a multi-RIS-aided point-to-point transmission assuming that the direct link does not exist and only the best RIS is selected to participate in the transmission. Assuming that all the Rayleigh fading channels between different RISs are i.i.d., the authors showed that the e2e SNR approximately follows a non-central chi-square distribution. In [16], considering a multi-RIS-aided system, in which the number of elements of each RIS can be arbitrarily adjusted, the authors proposed RIS selection strategies based on the RISs' location information. The performance analysis was carried out based on the assumption that the magnitudes of the channel coefficients associated with different RISs are i.i.d. RVs. In [17], considering multi-hop multi-RIS-aided systems, the authors proposed a RIS selection strategy that maximizes the e2e SNR. However, the authors only took into account the impact of path-loss and ignored the impact of fading. In [18], the authors discussed the impact of the centralized and distributed RIS deployment strategies on the capacity region of multi-RIS-aided systems. However, in the distributed RIS deployment, the authors assumed that the channels associated with the different distributed RISs underwent i.i.d. Rayleigh fading. In [19], the authors considered multi-RIS-aided systems for both indoor and outdoor communications, where a direct link between a source and a destination is unavailable; aiming for low-complexity transmission, the authors proposed a RIS selection strategy that selects the RIS with the highest SNR to assist the communication. However, small-scale fading was ignored and the performance analysis of the RIS selection strategy was not carried out.

Although previous works have provided important contributions to multi-RIS-aided systems, the accurate characterization of the fading model is still an open problem. Specifically, to facilitate the performance analysis, some existing works only considered path-loss effects and/or ignored small-scale fading effects, as in [17]–[19]. On the other hand, when taking into account small-scale fading, existing works relied on the i.i.d. fading channel model [4], [15], and [18] or deterministic fading channel, as in [14]. Channels associated with different elements of the same RIS can be reasonably assumed to be i.i.d. as aforementioned since the elements are typically in sub-wavelength size [1] and are installed closely to each other on the same panel. However, channels between different RISs cannot be assumed to be i.i.d., because in distributed multi-RIS-aided systems, the RISs are installed significantly far apart, e.g., tens of meters.

Motivated by the aforementioned observations, in this work, we propose two distributed multi-RIS-aided wireless schemes, namely, the exhaustive RIS-aided (ERA) and opportunistic RIS-aided (ORA) schemes. Specifically, in the former, all the RISs participate in the transmission, whereas in the later, only one scheduled RIS is employed. It is shown that both approaches have their own advantages and drawbacks. In particular, the ERA scheme may give better performance at the expense of additional complexity and fronthaul/backhaul load. On the other hand, by using only one RIS, as in the ORA scheme, the other RISs can be employed for other purposes (assisting other pairs of users, for instance), consequently providing a more efficient use of the available resources. Thus, depending on the needs and goals of the application, one approach can be more useful than the other. Considering such multi-RIS-aided schemes, we raise a research question that still needs to be properly answered in the literature: *what distributions can be used to model the magnitude of the e2e channel coefficient of distributed multi-RIS-aided systems, which is a combination of direct and all reflecting channel coefficients?* Thus, to answer the raised research question comprehensively, we consider a practical multi-RIS-aided system setting, in which channels associated with reflecting elements of the same RIS are assumed to be i.i.d., whereas channels associated with different RISs are assumed to be independent but not identically distributed (i.n.i.d.), and the system undergoes Nakagami-m fading. The key contributions of this work are summarized as follows:

- We prove that the distribution of the magnitude of the e2e channel coefficient of the ERA scheme can be approximated by either a Gamma distribution or a LogNormal distribution. On the other hand, the magnitude of the e2e channel coefficient of the ORA scheme can be approximated by a LogNormal distribution. It is noteworthy that these findings have not yet been reported in the literature.
- For the system performance analysis, invoking the above findings, tight approximate closed-form expressions for the outage probability (OP) and ergodic capacity (EC) of the ERA and the ORA schemes are derived, based on which insightful discussions are drawn. Specifically, we show that the approximation based on Gaussian distribution, as in [6] and [11] for single-RIS-aided systems and [4], [14], and [15] for multi-RIS-aided systems, is no longer an appropriate method for i.n.i.d. fading channels, because the Gaussian approximation results in a tangible gap between the true OP and the approximate OP.
- From an engineering (and system design) perspective, our results reveal that the ERA scheme outperforms the ORA scheme in terms of OP and EC; nevertheless, the ORA scheme achieves a higher energy efficiency (EE) in a specific range of the target spectral efficiency (SE) under a certain network setting. From the system infrastructure viewpoint, the number of elements installed at each RIS and the locations of the RISs have significant impacts on the performance of the proposed schemes, in which, the ERA scheme is more robust against the change of the system infrastructure than the ORA scheme. We show that both centralized and distributed multi-RIS-

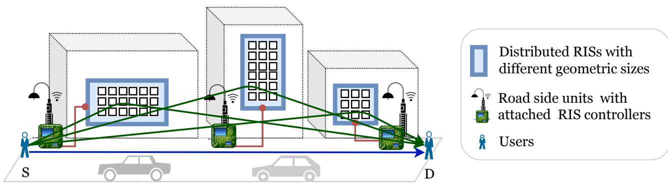

Fig. 1. Illustrations of a distributed multi-RIS-aided wireless system, where RISs can be installed on houses and/or buildings.

aided systems have their own advantages and drawbacks, which depends on the pre-planed locations of RISs. It is noted that to provide a reproducible research, our simulation code has been made available in [20].

The remainder of this paper is structured as follows. In Section II, we describe the system model and the channel model for the ERA and the ORA schemes. In Sections III and IV, we present the performance analysis of the ERA and the ORA schemes, respectively. In Section V, illustrative numerical results are plotted to corroborate the proposed fading models as well as to provide further insights into the system performance. Finally, Section VI concludes the paper. **Notations**: $\Gamma(\cdot)$ denotes the Gamma function [21, Eq. (8.310.1)], $\gamma(\cdot,\cdot)$ denotes the lower incomplete Gamma function [21, Eq. (8.350.1)], $K_\nu(z)$ denotes the modified Bessel function of the second kind [21, Eq. (8.407.1)], $\ln(x) = \log_e(x)$, $\mathrm{erf}(\cdot)$ denotes the error function [22, Eq. (7.1.1)], $G_{p,q}^{m,n}[\cdot]$ denotes the Meijer-G function [23, Eq. (8.2.1.1)]. $X \overset{\text{approx.}}{\sim} \mathcal{D}(\cdot)$ means X approximately follows the distribution $\mathcal{D}(\cdot)$. For parameters of distributions, e.g., α_X means the parameter α in the distribution of random variable X, $\mu_X(k)$ denotes the k-th moment of X, and $F_A(\cdot)$ denotes the Lauricell function Type-A [24, Eq.(1.4.1)].

II. System Model

We consider a distributed multi-RIS-aided system, consisting of one source, S, that communicates with one destination, D, through a direct link with the assistance of N distributed RISs, $\mathrm{R}_n, n = 1, ..., N$, as depicted in Fig. 1. It is assumed that S and D are single-antenna nodes, whereas the n-th RIS is equipped with L_n passive reflecting elements. It is noted that the RISs may have different geometric sizes, i.e., $L_i \neq L_j, i, j \in \{1, ..., N\}$. Let $\mathbf{\Theta}_n = \mathrm{diag}(\kappa_{n1}e^{j\theta_{n1}}, ..., \kappa_{nl}e^{j\theta_{nl}}, ..., \kappa_{nL_n}e^{j\theta_{nL_n}})$ denote the phase-shift matrix [25], where $\kappa_{nl} \in (0, 1]$ and θ_{nl} stand for, respectively, the amplitude reflection coefficient and the phase-shift of the l-th reflecting element of the n-th RIS. Each RIS is programmed by a dedicated controller, where the controllers can be connected via a high-speed backhaul to synchronize the phase-shift configuration over the entire system.

Let $\tilde{h}_{nl}$ and $\tilde{g}_{nl}$ denote the *complex channel coefficients* from S to the l-th reflecting element of the n-th RIS, and from that reflecting element to D, respectively; and let $\tilde{h}_0$ denote channel coefficient of the direct $\mathrm{S} \to \mathrm{D}$ link. Knowing that, for a complex number z, one can represent $z = r(\cos\theta - j\sin\theta) = re^{-j\theta}$, where $\theta = \arg z$ and $r = |z|$, and $|re^{j\theta}| = |re^{-j\theta}|, \forall r \in \mathbb{R}$, the channels can be expressed in their polar representations as $\tilde{h}_0 = h_0 e^{-j\phi_0}$, $\tilde{h}_{nl} = h_{nl}e^{-j\phi_{nl}}$, $\tilde{g}_{nl} = g_{nl}e^{-j\psi_{nl}}$, where h_0, h_{nl}, and g_{nl} are *the magnitudes of the channel coefficients*, i.e., $h_0 = |\tilde{h}_0|$, $h_{nl} = |\tilde{h}_{nl}|$, and $g_{nl} = |\tilde{g}_{nl}|$, and ϕ_0, ϕ_{nl}, and ψ_{nl} are *the phases* of $\tilde{h}_0$, $\tilde{h}_{nl}$, and $\tilde{g}_{nl}$, respectively, with $\{\phi_0, \phi_{nl}, \psi_{nl}\} \in [0, 2\pi]$. Let x_S, with $\mathbb{E}[|x_\mathrm{S}|^2] = 1$, be the transmit symbol at S, P_S be the transmit power (in [dBm]) of S, and w_D be the additive white Gaussian noise (AWGN) at D with zero mean and variance σ_D^2, i.e., $w_\mathrm{D} \sim \mathcal{CN}(0, \sigma_\mathrm{D}^2)$.

A. The Exhaustive RIS-aided Scheme

In the ERA scheme, all the RISs assist the transmission between S and D, i.e., when S transmits its signal x_S to D, all N RISs are controlled to reflect replicas of x_S to D over the same time-frequency channel. Herein, we assume that all RISs are controlled to steer their beams to the destination, and therefore they cannot interfere with each other, as in [4], [15], [16], and [19]. As a result, D receives a superposition (combination) of the all received multi-path signals. Thus, using coherent combination [4] and [13], the received signal at D, which is synthesized from the direct signal and reflected signals from all N RISs, can be written as

$$y^{\mathrm{ERA}} = \sqrt{P_\mathrm{S}}\left(\tilde{h}_0 + \sum_{n=1}^{N}\sum_{l=1}^{L_n} \tilde{g}_{nl}\kappa_{nl}e^{j\theta_{nl}}\tilde{h}_{nl}\right)x_\mathrm{S} + w_\mathrm{D}. \quad (1)$$

Using polar representation of the complex channel coefficients, the received SNR at D can be expressed as

$$\begin{aligned}&\mathrm{SNR}^{\mathrm{ERA}} \\ &= \bar{\rho}\left|h_0 e^{-j\phi_0} + \sum_{n=1}^{N}\sum_{l=1}^{L_n} g_{nl}\kappa_{nl}h_{nl}e^{j(\theta_{nl}-\phi_{nl}-\psi_{nl})}\right|^2 \quad (2)\\ &= \bar{\rho}\underbrace{|e^{-j\phi_0}|^2}_{=1}\left|h_0 + \sum_{n=1}^{N}\sum_{l=1}^{L_n} g_{nl}\kappa_{nl}h_{nl}e^{j\delta_{nl}}\right|^2, \quad (3)\end{aligned}$$

where $\bar{\rho} = P_\mathrm{S}/\sigma_\mathrm{D}^2$ denotes the *average transmit SNR* [dB] and $\delta_{nl} \triangleq \theta_{nl} - \phi_{nl} - \psi_{nl} + \phi_0$ is *the phase error* of the l-th reflecting element of the n-th RIS.

In order to overcome the destructive effect of multi-path fading, the phase-shifts of the RISs are reconfigured such that all the received signals are constructively added to achieve the largest SNR. Mathematically, the ideal phase-shift configuration of the l-th reflecting element of the n-th RIS can be expressed as

$$\theta_{nl}^* = \arg\max_{\theta_{nl}\in\mathcal{Q}_n} \mathrm{SNR}^{\mathrm{ERA}}(\theta_{nl}), \forall l, \forall n. \quad (4)$$

In practice, considering discrete phase-shifts, the number of phase-shifts is limited and constrained by a phase-shift resolution, which is the number of quantization bits, b_n, for the n-th RIS. Let $Q_n \triangleq 2^{b_n}$ denote the phase-shift resolution of the n-th RIS. Thus, the value of a phase-shift can be picked from the following set $\mathcal{Q}_n = \left\{0, \frac{2\pi}{Q_n}, \frac{4\pi}{Q_n}, ..., \frac{2\pi(Q_n-1)}{Q_n}\right\}$ [26]. Assuming a high phase-shift resolution, i.e., $2^{b_n} \gg 1$, and perfect channel state information (CSI), the n-th RIS is able to generate ideal phase-shifts such that the phase errors can be zero, i.e., $\delta_{nl} = 0, \forall l, \forall n$. It is noted that the ideal phase-shift assumption has been extensively used for single-RIS-aided systems [6], [11], [12], [27], and [9], multi-RIS-aided systems [4] and [15], and multi-hop multi-RIS-aided networks [17]. As a result, $\theta^*_{nl} = (\phi_{nl} + \psi_{nl}) - \phi_0$, which yields a synthesized received signal at D having the largest amplitude. Thus, the received SNR at D can be re-expressed as

$$\mathrm{SNR}^{\mathrm{ERA}} = \bar{\rho}\left|h_0 + \sum_{n=1}^{N}\sum_{l=1}^{L_n}\kappa_{nl}h_{nl}g_{nl}\right|^2. \tag{5}$$

B. The Opportunistic RIS-aided Scheme

Instead of using all the RISs, we propose the ORA scheme with the aim to reduce the resource usage. In this case, only the most appropriate RIS participates in assisting the direct transmission. The benefit of the ORA scheme is that it provides a low-complexity and energy-efficient transmission protocol at the receiver side. Consequently, the receiver in the ORA scheme handles a significantly lower number of reflecting signals compared to the ERA scheme. Specifically, assuming that the n-th RIS is scheduled to assist the direct transmission, the received signal at D can be written as

$$y_n^{\mathrm{ORA}} = \sqrt{P_{\mathrm{S}}}\left(\tilde{h}_0 + \sum_{l=1}^{L_n}\tilde{g}_{nl}\kappa_{nl}e^{j\theta_{nl}}\tilde{h}_{nl}\right)x_{\mathrm{S}} + w_{\mathrm{D}}. \tag{6}$$

The received SNR associated with the n-th RIS can be expressed as

$$\mathrm{SNR}_n^{\mathrm{ORA}} = \bar{\rho}\underbrace{|e^{-j\phi_0}|^2}_{=1}\left|h_0 + \sum_{l=1}^{L_n}g_{nl}\kappa_{nl}h_{nl}e^{j\delta_{nl}}\right|^2, \tag{7}$$

where $\delta_{nl} = \theta_{nl} - \phi_{nl} - \psi_{nl} + \phi_0$. In the ORA scheme, the selected RIS is the one that potentially provides the highest e2e received SNR at D. Specifically, the opportunistic scheduling criterion to choose the most appropriate RIS can be mathematically expressed as

$$n^* = \arg\max_{1\le n\le N}\max_{\theta_{nl}\in\mathfrak{Q}_n}\mathrm{SNR}_n^{\mathrm{ORA}}, \forall l, \forall n. \tag{8}$$

In order to meet (8), the ideal phase-shift configuration is first estimated at each reflecting element of each RIS, i.e., $\theta^*_{nl} = (\phi_{nl}+\psi_{nl})-\phi_0, \forall l, \forall n$. Thus, the criterion (8) can be rewritten as $n^* = \arg\max_{1\le n\le N}\mathrm{SNR}_n^{\mathrm{ORA}}$, i.e.,

$$\begin{aligned}\mathrm{SNR}_{n^*}^{\mathrm{ORA}} &= \max_{1\le n\le N}\mathrm{SNR}_n^{\mathrm{ORA}}\\ &= \max_{1\le n\le N}\left\{\bar{\rho}\left|h_0 + \sum_{l=1}^{L_n}g_{nl}\kappa_{nl}h_{nl}\right|^2\right\}. \end{aligned} \tag{9}$$

As can be observed, the operation of the ORA scheme requires the same number of CSI estimations as required by the ERA scheme. Nevertheless, the destination node in the ORA scheme just needs to process $(L_n + 1)$ received signals compared to $(N \times L_n + 1)$ signals in the ERA scheme. This difference in the participating passive elements results in a significant gap between the EE of the two schemes.

III. Performance Analysis of the ERA Scheme

For notational simplicity, along the analysis, let $U_{nl} \triangleq \kappa_{nl}h_{nl}g_{nl}$, $V_n \triangleq \sum_{l=1}^{L_n}U_{nl}$, $M_V \triangleq \max_{1\le n\le N}V_n$, $T \triangleq \sum_{n=1}^{N}V_n$, $Z \triangleq h_0 + T$, and $R \triangleq h_0 + M_V$.

A. The Proposed Framework for Statistical Characterization of the Magnitude of the e2e Channel

The magnitudes of the e2e channel coefficients in the ERA and the ORA schemes can be represented by the RVs Z and R, respectively. Directly deriving true distributions of these RVs is infeasible because of their complicated structures. For instance, in the ERA scheme, Z consists of N i.n.i.d. RVs, where each of these i.n.i.d. RVs consists of $2L_n$ i.i.d. RVs. To deal with this technical problem, we propose a methodology to determine an approximate version of the true distribution. The 3-step framework is proposed as follows:

- Step 1: We first determine which parametric distribution is the best candidate to approximate the true distribution. Specifically, we heuristically and numerically match the *simulated true distribution* to some known candidate distributions, e.g., Gamma distribution, LogNormal distribution, Gaussian distribution, Burr distribution, Weibull distribution, just to name of few, by using the fitdist function of Matlab [28]. We then select the best candidate distributions, which give a high goodness of fit and accurate simulation results of performance metrics of interests, e.g., outage probability (OP) and/or ergodic capacity (EC), as will be shown in Theorems 1, 2, and 4. If no appropriate candidate distribution can be found, we focus on matching the simulated true distribution of a key component of the considered RV to the known candidate distribution, as will be shown in Theorem 3.
- Step 2: We next determine the statistical characteristics, i.e., parameters, of the candidate parametric distribution using *the method of moments* [29]. In particular, based on the knowledge of the statistical characteristics of the true distribution of individual components, e.g., the k-th moment of the Nakagami-m distribution of each individual channel, we determine the probability distribution and the associated parameters of the candidate distribution that best fits the statistical characteristics of the magnitude of the e2e channel coefficient. The key derivation is to determine *the method of moments estimators* of the parameters of the candidate distribution. More specifically, to derive the estimators, we match the first k moments of the candidate distribution, which are unknown, with that of the simulated true distribution, which are known as *population moments* and can be derived, to form a system of equations that can be solved to find the representation of the estimators. For instance, if the candidate distribution of the magnitude of the e2e channel coefficient is postulated to be a parametric Gamma distribution with the PDF given in (12), the tricky part is how to determine the estimators for the parameters α and β of this Gamma distribution, e.g., solve the system of equations and find the k-th moment of the simulated true distribution, such that this distribution can accurately characterize the true distribution of the magnitude of the e2e channel coefficient.
- Step 3: We verify the accuracy of the obtained approximate distribution. Specifically, in order to evaluate the accuracy of the obtained statistical model, we rely on the

corroboration between the simulated true distribution and the matched distribution.

Next, we present some essential distributions, which will be used along the performance analysis. Let X be a RV following a Nakagami-m distribution with its PDF and CDF, parameterized by m and Ω, given by [30]

$$f_X(x;m,\Omega)=\frac{2m^m}{\Gamma(m)\Omega^m}x^{2m-1}e^{-\frac{m}{\Omega}x^2}, x\geq 0, \tag{10}$$

$$F_X(x;m,\Omega)=\frac{\gamma\left(m,\frac{m}{\Omega}x^2\right)}{\Gamma(m)}, x\geq 0. \tag{11}$$

Here, $m>0$ is the *shape parameter*, indicating the severity of fading and $\Omega>0$ is the *spread parameter* of the distribution. Next, we use the alternative representation for denoting a Nakagami-m RV: $X\sim \text{Nakagami}(m,\Omega)$. It is noted that Ω denotes the mean square value of X, i.e., $\Omega=\mathbb{E}[X^2]$ [31], which is equivalent to the average channel (power) gain. The distribution of the magnitude of each individual channel can be expressed as $h_0\sim \text{Nakagami}(m_0,\Omega_0)$, $h_{nl}\sim \text{Nakagami}(m_{\text{h}_n},\Omega_{\text{h}_n})$, and $g_{nl}\sim \text{Nakagami}(m_{\text{g}_n},\Omega_{\text{g}_n})$, where $l=1,...,L_n$ and $n=1,...,N$.

Let Y be a RV following a Gamma distribution, whose PDF and CDF, parameterized by α and β, respectively given by [30]

$$f_Y(y;\alpha,\beta)=\frac{\beta^\alpha}{\Gamma(\alpha)}y^{\alpha-1}e^{-\beta y}, y\geq 0, \tag{12}$$

$$F_Y(y;\alpha,\beta)=\frac{\gamma(\alpha,\beta y)}{\Gamma(\alpha)}, y\geq 0. \tag{13}$$

Here, $\alpha>0$ is the *shape parameter* and $\beta>0$ is the *rate parameter* of the distribution. Hereafter, we use the following representation to denote a Gamma RV: $Y\sim\text{Gamma}(\alpha,\beta)$.

Let W be a RV following a LogNormal distribution, whose PDF and CDF are given by [30]

$$f_W(w;\nu,\zeta)=\frac{1}{w\sqrt{2\pi\zeta^2}}e^{-\frac{(\ln w-\nu)^2}{2\zeta^2}}, w>0,\zeta>0, \tag{14}$$

$$F_W(w;\nu,\zeta)=\frac{1}{2}+\frac{1}{2}\text{erf}\left(\frac{\ln w-\nu}{\sqrt{2\zeta^2}}\right), \tag{15}$$

respectively, where ν and ζ^2 are the *mean* and the *variance* of the distribution of W. Hereafter, we use the following representation to denote a LogNormal RV: $W\sim\text{LogNormal}(\nu,\zeta)$.

B. Statistical Channel Characterization of the ERA Scheme Based on Gamma Distribution

Relying on the proposed distribution estimation framework, we show that the true distribution of Z can be accurately approximated by the Gamma distribution, as shown in Theorem 1.

Theorem 1. *The true distribution of Z can be approximated by the Gamma distribution, which is characterized by two parameters α_Z and β_Z, i.e.,*

$$Z\overset{\text{approx.}}{\sim}\text{Gamma}(\alpha_Z,\beta_Z), \tag{16}$$

where the estimators of α_Z and β_Z can be expressed as

$$\alpha_Z=\frac{(\mathbb{E}[Z])^2}{\text{Var}[Z]}=\frac{[\mu_Z(1)]^2}{\mu_Z(2)-[\mu_Z(1)]^2}, \tag{17}$$

$$\beta_Z=\frac{\mathbb{E}[Z]}{\text{Var}[Z]}=\frac{\mu_Z(1)}{\mu_Z(2)-[\mu_Z(1)]^2}, \tag{18}$$

respectively, where $\mu_Z(1)$ and $\mu_Z(2)$ are presented in (80) *and* (81)*, respectively. Thus, the approximate PDF and CDF of Z, i.e., $f_Z(z;\alpha_Z,\beta_Z)$ and $F_Z(z;\alpha_Z,\beta_Z)$, can be expressed using* (12) *and* (13)*, respectively.*

Proof: The proof is provided in Appendix A. ■

It is worth noting that the tricky part is to determine the statistical characteristics of the Gamma distribution, i.e., $\mu_Z(1)$ and $\mu_Z(2)$. In addition, knowing that for arbitrary X and Y, where $Y=cX^2$, we have $F_Y(y)=F_X(\sqrt{y/c})$ and $f_Y(y)=\frac{1}{2\sqrt{cy}}f_X\left(\sqrt{\frac{y}{c}}\right)$, the PDF and CDF of Z^2 can be obtained as

$$f_{Z^2}(x)\approx\frac{1}{2\sqrt{x}}\frac{{\beta_Z}^{\alpha_Z}}{\Gamma(\alpha_Z)}\left(\sqrt{x}\right)^{\alpha_Z-1}e^{-\beta_Z\sqrt{x}}, \tag{19}$$

$$F_{Z^2}(x)\approx\frac{\gamma\left(\alpha_Z,\beta_Z\sqrt{x}\right)}{\Gamma(\alpha_Z)}, \tag{20}$$

respectively. On the other hand, the PDF and CDF of the Generalized Gamma distribution are, respectively, given by [32]

$$f_{\text{GG}}(x;a,d,p)=\frac{\left(p/a^d\right)x^{d-1}e^{-\left(\frac{x}{a}\right)^p}}{\Gamma\left(d/p\right)}, \tag{21}$$

$$F_{\text{GG}}(x;a,d,p)=\frac{\gamma\left(d/p,(x/a)^p\right)}{\Gamma(d/p)}, \tag{22}$$

where a,d,p are parameters of the distribution. Thus, (19) can be rewritten using (21) as

$$f_{Z^2}(x)=\frac{[1/2]/\left[\left(\beta_Z^{-2}\right)^{\frac{\alpha_Z}{2}}\right]}{\Gamma([\alpha_Z/2]/[1/2])}x^{\frac{\alpha_Z}{2}-1}e^{-\left(\frac{x}{\beta_Z^{-2}}\right)^{\frac{1}{2}}}, \tag{23}$$

Next, we present the statistical characterization of the *e2e channel power gain* of the ERA scheme. By comparing (21) and (23), the distribution functions of Z^2 can be represented in the form of the Generalized Gamma distribution as in the following Remark 1.

Remark 1. *From Theorem 1, the true distribution of Z^2 can be approximated by using the Generalized Gamma distribution, where the PDF and CDF of Z^2 can be expressed as*

$$f_{Z^2}(x)=f_{\text{GG}}\left(x;a_{Z^2},d_{Z^2},p_{Z^2}\right), \tag{24}$$

$$F_{Z^2}(x)=F_{\text{GG}}\left(x;a_{Z^2},d_{Z^2},p_{Z^2}\right), \tag{25}$$

respectively, where $f_{\text{GG}}(\cdot)$ and $F_{\text{GG}}(\cdot)$ are presented in (21) *and* (22)*, respectively, $a_{Z^2}=\beta_Z^{-2}$, $d_{Z^2}=\alpha_Z/2$, and $p_{Z^2}=1/2$, where α_Z and β_Z are expressed in* (17) *and* (18)*, respectively.*

Next, relying on Theorem 1, we evaluate the performance of the ERA scheme in terms of OP and EC.

1) Outage Probability: The OP can be defined as the probability that the instantaneous mutual information of the ERA scheme drops below a target SE threshold R_{th} [b/s/Hz], i.e., $P_{\text{out}}^{\text{ERA}} = \Pr(\log_2(\text{SNR}^{\text{ERA}}+1) < R_{\text{th}})$. From (5), and invoking Theorem 1, an approximate closed-form expression for the OP of the ERA scheme can be obtained as

$$\begin{aligned} P_{\text{out}}^{\text{ERA,Gam}} &= \Pr\left(\bar{\rho}Z^2 \le \rho_{\text{th}}\right) \\ &\overset{\text{(a)}}{\approx} F_Z\left(\sqrt{\rho_{\text{th}}/\bar{\rho}}\right), \end{aligned} \tag{26}$$

where $\rho_{\text{th}} = 2^{R_{\text{th}}} - 1$ and step (a) in (26) is due to the fact that $F_{X^2}(x) = F_X(\sqrt{x}), x > 0$.

2) Ergodic Capacity: The system ergodic capacity can be determined by averaging the system instantaneous capacity over a large number of channel realizations. Invoking Theorem 1, an approximate closed-form expression for the EC of the ERA scheme can be expressed as

$$\begin{aligned} \bar{C}^{\text{ERA,Gam}} &= \mathbb{E}\left[\log_2\left(1+\text{SNR}^{\text{ERA}}\right)\right] \\ &= \mathbb{E}\left[\log_2\left(1+\bar{\rho}Z^2\right)\right] \\ &\approx \frac{1}{\Gamma(\alpha_Z)\ln 2}\frac{2^{\alpha_Z-1}}{\sqrt{\pi}} \\ &\quad\times G_{3,5}^{5,1}\left(\frac{(\beta_Z)^2}{4\bar{\rho}}\middle|\begin{matrix}0,\frac{1}{2},1\\ \frac{\alpha_Z}{2},\frac{\alpha_Z+1}{2},0,\frac{1}{2},0\end{matrix}\right). \end{aligned} \tag{27}$$

The detailed derivation of (27) is provided in Appendix B.

C. Statistical Channel Characterization of the ERA Scheme Based on LogNormal Distribution

Next, we show that the LogNormal distribution can alternatively be used to approximate the true distribution of the magnitude of the e2e channel coefficient of the ERA scheme.

Theorem 2. *The true distribution of Z can be approximated by the LogNormal distribution, which is characterized by two parameters ν_Z and ζ_Z, i.e.,*

$$Z \overset{\text{approx.}}{\sim} \text{LogNormal}(\nu_Z, \zeta_Z), \tag{28}$$

where the estimators of ν_Z and ζ_Z are given in (29) *and* (30)*, respectively.*

Proof: Since the LogNormal distribution is characterized by two parameters ν and ζ, following Step 2 of our framework, we need to match the first two moments of Z, i.e., solving the following system of equations: $\mathbb{E}[Z] = \mathbb{E}[X]$ and $\mathbb{E}[Z^2] = \mathbb{E}[X^2]$, where X is a LogNormal RV. As a result, the estimators of ν_Z and ζ_Z can be written as [33]

$$\nu_Z = \ln\left(\frac{(\mathbb{E}[Z])^2}{\sqrt{\mathbb{E}[(Z)^2]}}\right) = \ln\left(\frac{(\mu_Z(1))^2}{\sqrt{\mu_Z(2)}}\right), \tag{29}$$

$$\zeta_Z = \sqrt{\ln\left(\frac{\mathbb{E}[Z^2]}{(\mathbb{E}[Z])^2}\right)} = \sqrt{\ln\left(\frac{\mu_Z(2)}{(\mu_Z(1))^2}\right)}. \tag{30}$$

Next, in order to determine the exact values of ν_Z and ζ_Z, we derive a general expression for the k-th moment of Z, i.e., $\mu_Z(k) = \mathbb{E}[Z^k]$. After some mathematical manipulations, $\mu_Z(k)$ can be obtained as

$$\begin{aligned} \mu_Z(k) &= \sum_{l=0}^{k}\binom{k}{l}\mathbb{E}[(h_0)^l]\mathbb{E}[T^{k-l}] \\ &= \sum_{l=0}^{k}\binom{k}{l}\mu_{h_0}(l)\mu_T(k-l), \end{aligned} \tag{31}$$

where $\mu_{h_0}(k)$ and $\mu_T(k)$ are derived in (64) and (76), respectively. Consequently, the PDF, $f_Z(x;\nu_Z,\zeta_Z)$, and the CDF, $F_Z(x;,\nu_Z,\zeta_Z)$, can be expressed using (14) and (15), respectively. This completes the proof of Theorem 2. ■

1) Outage Probability: An approximate closed-form expression for the OP of the ERA scheme can be obtained as

$$\begin{aligned} P_{\text{out}}^{\text{ERA,LN}} &= \Pr\left(\bar{\rho}Z^2 \le \rho_{\text{th}}\right) \\ &= F_Z\left(\sqrt{\frac{\rho_{\text{th}}}{\bar{\rho}}}\right) \\ &\approx \frac{1}{2} + \frac{1}{2}\text{erf}\left(\frac{\ln\left(\sqrt{\frac{\rho_{\text{th}}}{\bar{\rho}}}\right) - \nu_Z}{\sqrt{2\zeta_Z^2}}\right). \end{aligned} \tag{32}$$

2) Ergodic Capacity: The EC of the ERA scheme can be determined as $\bar{C}^{\text{ERA,LN}} = \mathbb{E}\left[\log_2\left(1+\bar{\rho}Z^2\right)\right]$.

Lemma 1. *Given $X \sim \text{LogNormal}(\nu_X, \zeta_X)$, and let $\bar{C}_X = \mathbb{E}\left[\log_2\left(1+\bar{\rho}X\right)\right]$, it can be shown that $\bar{C}_X = \Upsilon(\nu_X, \zeta_X)$, where*

$$\begin{aligned} &\Upsilon(\nu_X,\zeta_X) \\ &\triangleq \frac{1}{\ln(2)}\Bigg[\Xi\left(\frac{1}{\zeta\sqrt{2}},\frac{\ln(\bar{\rho})+\nu}{\zeta\sqrt{2}}\right) + \Xi\left(\frac{1}{\zeta\sqrt{2}},-\frac{\ln(\bar{\rho})+\nu}{\zeta\sqrt{2}}\right) \\ &\quad + \frac{\zeta}{\sqrt{2\pi}}e^{-\frac{(\ln(\bar{\rho})+\nu)^2}{2\zeta^2}} + \frac{\ln(\bar{\rho})+\nu}{2}\text{erfc}\left(-\frac{\ln(\bar{\rho})+\nu}{\zeta\sqrt{2}}\right)\Bigg]. \end{aligned} \tag{33}$$

Here, $\Xi(\cdot,\cdot)$ is derived in (38).

Proof: We have

$$\begin{aligned} \bar{C}_X &= \mathbb{E}\left[\log_2\left(1+\bar{\rho}X\right)\right] \\ &= \int_0^\infty \log_2(1+x)\frac{1}{\bar{\rho}}f_X\left(\frac{x}{\bar{\rho}}\right)dx. \end{aligned} \tag{34}$$

Substituting (14) into (34) yields

$$\bar{C}_X = \frac{1}{\bar{\rho}\zeta\sqrt{2\pi}}\int_0^\infty \frac{\log_2(1+x)}{x/\bar{\rho}}e^{-\frac{(\ln(x/\bar{\rho})-\nu)^2}{2\zeta^2}}dx. \tag{35}$$

Since $\log_2(1+x) = \ln(1+x)/\ln(2)$, we have

$$\bar{C}_X = \frac{1}{\zeta\sqrt{2\pi}\ln(2)}\int_0^\infty \frac{\ln(1+x)}{x}e^{-\frac{[\ln(x)-(\ln(\bar{\rho})+\nu)]^2}{2\zeta^2}}dx. \tag{36}$$

Following [34, Subsection II-A], one can arrive at the approximate closed-form expression for $\bar{C}_X$ in (33), where $\Xi(\cdot,\cdot)$ is defined as

$$\Xi(a,b) \triangleq \frac{a}{\sqrt{\pi}}\int_0^1 \frac{\ln(1+x)}{x}e^{-[a\ln(x)-b]^2}dx. \tag{37}$$

With some mathematical manipulations, the integral in (37) can be approximated by

$$\Xi(a,b) \approx \frac{e^{-b^2}}{2} \sum_{1\leq k\leq 8} a_k \mathrm{erfcx}\left(\frac{k}{2a}+b\right), \quad (38)$$

where $\mathrm{erfcx}(\cdot) = e^{x^2}\mathrm{erfc}(\cdot)$. This completes the proof of Lemma 1. ■

Based on $Z \overset{\text{approx.}}{\sim} \mathrm{LogNormal}(\nu_Z, \zeta_Z)$ as stated in Theorem 2, we can derive the PDF of Z^2, however, the resultant PDF of Z^2 using this method leads to a non-closed-form expression of the integral in (34). To circumvent this problem, we perform Step 2 of the proposed statistic characterization framework again, and after some mathematical manipulation steps, we obtain

$$Z^2 \overset{\text{approx.}}{\sim} \mathrm{LogNormal}(\nu_{Z^2}, \zeta_{Z^2}),$$

where

$$\nu_{Z^2} = \ln\left(\frac{(\mu_{Z^2}(1))^2}{\sqrt{\mu_{Z^2}(2)}}\right),$$
$$\zeta_{Z^2} = \sqrt{\ln\left(\frac{\mu_{Z^2}(2)}{(\mu_{Z^2}(1))^2}\right)},$$

and

$$\mu_{Z^2}(k) = \sum_{l=0}^{2k} \binom{2k}{l} \mu_{h_0}(l)\mu_T(2k-l).$$

Alternatively, we have

$$\nu_{Z^2} = \ln\left(\frac{(\mu_Z(2))^2}{\sqrt{\mu_Z(4)}}\right),$$
$$\zeta_{Z^2} = \sqrt{\ln\left(\frac{\mu_Z(4)}{(\mu_Z(2))^2}\right)}.$$

From (34), an approximate closed-form expression for the EC of the ERA scheme can be obtained as

$$\bar{C}^{\mathrm{ERA,LN}} = \mathbb{E}\left[\log_2\left(1+\bar{\rho}Z^2\right)\right] \approx \Upsilon(\nu_{Z^2}, \zeta_{Z^2}). \quad (39)$$

IV. Performance Analysis of the ORA Scheme

A. Statistical Channel Characterization of the ORA Scheme

We first rely on the proposed framework to match the true distribution of the key component of R, i.e., V_n, to a Gamma distribution, as stated in (72), and then we derive approximate closed-form expressions for the PDF and CDF of R. Specifically, since h_0 and V_n are independent RVs and $h_0, V_n \geq 0$, the opportunistic scheduling criterion in (8) can be re-expressed as

$$\begin{aligned} n^* &= \arg\max_{1\leq n\leq N} \left\{\bar{\rho}\left[h_0+V_n\right]^2\right\} \\ &= \arg\max_{1\leq n\leq N} V_n. \end{aligned} \quad (40)$$

Thus, the e2e SNR of the ORA scheme in (9) can be rewritten as

$$\mathrm{SNR}_{n^*}^{\mathrm{ORA}} = \bar{\rho}\left[h_0+M_V\right]^2, \quad (41)$$

The statistical characterization of the magnitude of the e2e channel coefficient of the ORA scheme is presented in the following theorem.

Theorem 3. *Approximate closed-form expressions for the CDF and PDF of R can be, respectively, obtained as in* (42) *and* (43)*, where $f_{h_0}(\cdot)$, $F_{h_0}(\cdot)$, and $F_{M_V}(\cdot)$ are presented in* (10), (11), *and* (52), *respectively.*

Proof: Since the $\max\{\cdot\}$ operation on V_n changes the statistical characteristics of its argument, V_n, we first rely on the Total Probability Theorem [30] and the definition of conditional probability [30] to determine the probability distribution of R. The CDF of R, $F_R(x)$, can be expressed as

$$F_R(x) = \Pr(R \leq x) = \Pr((h_0+M_V) \leq x). \quad (44)$$

From (40) and (41), (44) can be further expressed as

$$\begin{aligned} F_R(x) &= \Pr((h_0+V_{n^*}) \leq x) \\ &= \sum_{n=1}^{N} \Pr(n^*=n)\Pr\left((h_0+V_{n^*}) \leq x \mid n^*=n\right). \end{aligned} \quad (45)$$

Using the Bayes Theorem [30], we have

$$\begin{aligned} &\Pr\left((h_0+V_{n^*}) \leq x \mid n^*=n\right) \\ &= \frac{\Pr(\{(h_0+V_{n^*}) \leq x\} \cap \{n^*=n\})}{\Pr(n^*=n)}. \end{aligned} \quad (46)$$

Thus, (45) can be rewritten as

$$F_R(x) = \sum_{n=1}^{N} \Pr(\{(h_0+V_{n^*}) \leq x\} \cap \{n^*=n\}). \quad (47)$$

From (9) and (40), (47) can be further expressed as

$$F_R(x) = \sum_{n=1}^{N} \Pr(\{(h_0+V_n) \leq x\} \cap \{V_n = \max_{1\leq k\leq N} V_k\}). \quad (48)$$

It is noted that $V_n = \max_{1\leq k\leq N} V_k, n=1,...,N$, are pairwise disjoint events, and

$$\sum_{n=1}^{N} \Pr\left(V_n = \max_{1\leq k\leq N} V_k\right) = 1. \quad (49)$$

Thus, for an arbitrary event A, relying on the Total Probability Theorem [30], we have

$$\sum_{n=1}^{N} \Pr\left(\left\{V_n = \max_{1\leq k\leq N} V_k\right\} \cap A\right) = \Pr(A). \quad (50)$$

Thus, (48) can be further expressed as

$$\begin{aligned} F_R(x) &= \Pr\left(\{\max_{1\leq k\leq N} V_k \leq (x-h_0)\} \cap \{h_0 < x\}\right) \\ &= \int_0^x F_{M_V}(x-y) f_{h_0}(y) dy. \end{aligned} \quad (51)$$

$$F_R(x) \approx \Phi(x) \triangleq \sum_{m=1}^{M} \left[F_{h_0}\left(\frac{m}{M}x\right) - F_{h_0}\left(\frac{m-1}{M}x\right) \right] F_{M_V}\left(\frac{M-m+1}{M}x\right). \tag{42}$$

$$\begin{aligned} f_R(x) \approx \Delta(x) \triangleq \sum_{m=1}^{M} \Bigg[& \left[\frac{m}{M} f_{h_0}\left(\frac{m}{M}x\right) - \frac{m-1}{M} f_{h_0}\left(\frac{m-1}{M}x\right) \right] F_{M_V}\left(\frac{M-m+1}{M}x\right) \\ & \times \frac{M-m+1}{M} \left(F_{h_0}\left(\frac{m}{M}x\right) - F_{h_0}\left(\frac{m-1}{M}x\right) \right) f_{M_V}\left(\frac{M-m+1}{M}x\right) \Bigg]. \end{aligned} \tag{43}$$

Since V_k, $k = 1, ..., N$, are i.n.i.d. RVs, from (73), the CDF of M_V can be derived as

$$\begin{aligned} F_{M_V}(x) &= \Pr\left(\max_{1\le k\le N} V_k \le x\right) \\ &= \prod_{k=1}^{N} F_{V_k}(x) \approx \prod_{k=1}^{N} \frac{\gamma(L_k \alpha_{U\,k}, \beta_{U\,k} z)}{\Gamma(L_k \alpha_{U\,k})}. \end{aligned} \tag{52}$$

Inserting (52) into (51) results in an integral that cannot be expressed in a closed-form. To address this problem, we further express (51) as

$$F_R(x) = \int_0^x \int_0^{x-y} f_{M_V}(z) f_{h_0}(y) dz dy. \tag{53}$$

Using the M-staircase approximation, (53) can be derived as

$$F_R(x) \overset{M\to\infty}{\approx} \sum_{m=1}^{M} \int_{\frac{m-1}{M}x}^{\frac{m}{M}x} f_{h_0}(y) \int_0^{\frac{M-m+1}{M}x} f_{M_V}(z) dz dy. \tag{54}$$

After some mathematical manipulations, (54) can be derived as (42). Next, by taking the derivative of (42), i.e., $f_{h_0}(x) = \frac{dF_{h_0}(x)}{dx}$, the PDF of R is obtained as in (43), while the PDF of M_V, $f_{M_V}(x)$, is derived by taking the derivative of (52). This completes the proof of Theorem 3. ■

1) Outage Probability: Invoking Theorem 3, an approximate closed-form expression for the OP of the ORA scheme can be obtained as

$$\begin{aligned} P_{\text{out}}^{\text{ORA,Gam}} &= \Pr(\bar{\rho} R^2 \le \rho_{\text{th}}) \\ &= F_{R^2}(\rho_{\text{th}}/\bar{\rho}) = F_R\left(\sqrt{\rho_{\text{th}}/\bar{\rho}}\right) \\ &\approx \Phi\left(\sqrt{\rho_{\text{th}}/\bar{\rho}}\right), \end{aligned} \tag{55}$$

where $\Phi(\cdot)$ is presented in (42).

2) Ergodic Capacity: An analytical closed-form expression for the EC of the ORA scheme can be expressed as

$$\begin{aligned} \bar{C}^{\text{ORA,Gam}} &= \mathbb{E}[\log_2(1 + \bar{\rho} R^2)] \\ &= \frac{1}{\ln 2} \int_0^\infty \frac{1}{z+1} \left[1 - F_R\left(\sqrt{\frac{z}{\bar{\rho}}}\right) \right] dz. \end{aligned} \tag{56}$$

With the PDF of R in (42), the integral in (56) does not admit a closed-form expression. Nevertheless, an approximate closed-form expression for the EC of the ORA scheme is obtained in subsection IV-B2.

B. Statistical Channel Characterization of the ORA Scheme Based on LogNormal Distribution

To give more insights into the ORA scheme's fading model, we next show that the true distribution of R can be approximated by a LogNormal distribution.

Theorem 4. *The true distribution of R can be approximated by the LogNormal distribution, which is characterized by two parameters ν_R and ζ_R, i.e.,*

$$R \overset{\text{approx.}}{\sim} \text{LogNormal}(\nu_R, \zeta_R), \tag{57}$$

where the estimators of ν_R and ζ_R are presented in (58) *and* (59)*, respectively.*

Proof: By using the same mathematical reasoning as in Subsection III-C, the parameters characterizing the LogNormal distribution of R can be obtained as

$$\nu_R = \ln\left(\frac{(\mathbb{E}[R])^2}{\sqrt{\mathbb{E}[R^2]}}\right) = \ln\left(\frac{(\mu_R(1))^2}{\sqrt{\mu_R(2)}}\right), \tag{58}$$

$$\zeta_R = \sqrt{\ln\left(\frac{\mathbb{E}[R^2]}{(\mathbb{E}[R])^2}\right)} = \sqrt{\ln\left(\frac{\mu_R(2)}{(\mu_R(1))^2}\right)}. \tag{59}$$

To obtain the value of ν_R and ζ_R, we derive the k-th moment of R, which can be obtained as

$$\mu_R(k) = \sum_{v=0}^{k} \binom{k}{v} \mu_{h_0}(v) \mu_{M_V}(k-v), \tag{60}$$

From the CDF of M_V in (52), an expression for $\mu_{M_V}(k)$ is derived in the following Lemma.

Lemma 2. *A tight approximate closed-form expression for the k-th moment of M_V can be obtained as in* (61).

Proof: The proof is provided in Appendix C. ■

Invoking Lemma 2, and then substituting (64) and (61) into (60), we obtain the closed-form expression for $\mu_R(k)$. This completes the proof of Theorem 4. ■

1) Outage Probability: An approximate closed-form expression for the OP of the ORA scheme can be obtained as

$$\begin{aligned} P_{\text{out}}^{\text{ORA,LN}} &= \Pr(\bar{\rho} R^2 \le \rho_{\text{th}}) \\ &= F_R\left(\sqrt{\frac{\rho_{\text{th}}}{\bar{\rho}}}\right) \\ &\approx \frac{1}{2} + \frac{1}{2}\text{erf}\left(\frac{\ln\left(\sqrt{\frac{\rho_{\text{th}}}{\bar{\rho}}}\right) - \nu_R}{\sqrt{2\zeta_R^2}}\right). \end{aligned} \tag{62}$$

$$\mu_{M_V}(k) = \left[\sum_{t=1}^{N} \beta_{U\,t}\right]^{-k} \left[\prod_{t=1}^{N} \chi_t^{L_t \alpha_{U_t}}\right] \sum_{n=1}^{N} \frac{\Gamma(\Lambda + k)}{\Gamma(L_n \alpha_{U_n})} \prod_{\substack{t=1\\ t\neq n}}^{N} \frac{1}{\Gamma(L_t \alpha_{U\,t} + 1)}$$
$$\times F_A^{(N-1)}\Bigg[\Lambda + k;\ \underbrace{1, ..., 1}_{(N-1)\text{ terms}};\underbrace{L_1 \alpha_{U\,1} + 1, ..., L_N \alpha_{U\,N} + 1}_{\text{exclude } (L_n \alpha_{U_n} + 1)};\underbrace{\chi_1, ..., \chi_N}_{\text{exclude } \chi_n}\Bigg]. \tag{61}$$

2) Ergodic Capacity: Using the same argument made in subsection III-C2, and after some mathematical manipulations, we obtain

$$R^2 \overset{\text{approx.}}{\sim} \text{LogNormal}(\nu_{R^2}, \zeta_{R^2}),$$

where

$$\nu_{R^2} = \ln\left(\frac{(\mu_{R^2}(1))^2}{\sqrt{\mu_{R^2}(2)}}\right),$$
$$\zeta_{R^2} = \sqrt{\ln\left(\frac{\mu_{R^2}(2)}{(\mu_{R^2}(1))^2}\right)},$$

and

$$\mu_{R^2}(k) = \sum_{v=0}^{2k} \binom{2k}{v} \mu_{h_0}(v) \mu_{M_V}(2k - v).$$

Alternatively, we have

$$\nu_{R^2} = \ln\left(\frac{(\mu_R(2))^2}{\sqrt{\mu_R(4)}}\right),$$
$$\zeta_{R^2} = \sqrt{\ln\left(\frac{\mu_R(4)}{(\mu_R(2))^2}\right)}.$$

Invoking Lemma 1, an approximate closed-form expression for the EC of the ORA scheme can be expressed as

$$\begin{aligned}\bar{C}^{\text{ORA,LN}} &= \mathbb{E}\left[\log_2\left(1 + \bar{\rho} R^2\right)\right] \\ &\approx \Upsilon(\nu_{R^2}, \zeta_{R^2}).\end{aligned} \tag{63}$$

V. Results and Discussions

In this section, we provide representative results on the PDFs and CDFs of Z and R, as well as the OP, EC, and energy efficiency (EE) of the ERA and the ORA schemes, not only to verify the correctness of the developed analysis, but also to give insights into the performance of the two schemes. It is noteworthy that the results in this section are reproducible using our Matlab code [20], in which we detail the coding of the analytical results, the obtained CDFs and PDFs, and especially the Lauricell function Type-A, $F_A(\cdot)$, used in (61). One of the technical contributions of our code is that we use symbolic computations in Matlab [28] to obtain highly accurate results, e.g., using variable-precision arithmetic (vpa functions) to obtain analytical results with 32 significant decimal digits of precision. The reason of using symbolic computations is that the analysis of multi-RIS-aided systems under i.n.i.d. fading channels involves a high number of RVs, especially, when the number of elements of each RIS is large, some non-symbolic operations of floating-point arithmetic in Matlab are invalid and return not-a-number (NaN) results.

Unless otherwise specified, the simulation parameters are set to the values provided in Table I, where the equivalent noise power at D is $\sigma_{\text{D}}^2 = N_0 + 10\log(\text{BW}) + \text{NF}$ [dBm]. Considering non-line-of-sight (NLoS) condition in the 3GPP Urban Micro (UMi) path-loss model [19], [35], and [25], the path-loss is integrated in the spread parameter of the Nakagami-m distribution as $\Omega_{\text{XY}} = G_{\text{X}} + G_{\text{Y}} - 22.7 - 26\log(f_c) - 36.7\log(d_{\text{XY}}/d_0)$ [dB], where d_{XY} [m] is the distance in two-dimensional Cartesian coordinate system, where $\text{X} \in \{\text{S}, \text{R}_1, ..., \text{R}_\text{N}\}$, $\text{Y} \in \{\text{R}_1, ..., \text{R}_\text{N}, \text{D}\}$, and d_0 [m] is the reference distance, herein, $d_0 = 1$ m. Let $\mathbf{L} \in \mathbb{R}^{1\times N}$ denote a vector that indicates the number of reflecting elements of each one of the N RISs, i.e., $\mathbf{L} = [L_n : n = 1, ..., N]$. We consider four reflecting element setting as follows: $\mathbf{L}_1 = [25, 25, 25, 25, 25]$, is used in Figs. 2-4, $\mathbf{L}_2 = [40, 40, 40, 40, 40]$, $\mathbf{L}_3 = [20, 30, 40, 50, 60]$, and $\mathbf{L}_4 = [60, 50, 40, 30, 20]$, which are used in Figs. 5-7. Let $\mathbf{D} \in \mathbb{R}^{1\times 2N} = [(x_{\text{R}_n}, y_{\text{R}_n}) : n = 1, ..., N]$ represent the coordinates of the RISs. We consider two location settings, namely $\mathbf{D}_1 = [(7, 2), (13, 6), (41, 8), (75, 4), (93, 3)]$, used in Figs. 2-7, and $\mathbf{D}_2 = [(5, 2), (13, 7), (37, 6), (69, 1), (91, 3)]$, used in Fig. 7.

In Figs. 2a and 2b, we examine the accuracy of the proposed statistical models in Theorems 1 and 3, and Theorems 2 and 4, respectively. As can be seen, the analytical approximate CDFs and PDFs are well corroborated with the true CDF and PDF (estimated numerically based on simulation data). In addition, as shown in Fig. 3, the analytical and simulation results for the OP and EC of the ERA and the ORA schemes are well corroborated, which validates the analysis in Theorems. 1-4.

In Fig. 4, we show that the use of Gamma and LogNormal distributions are indeed significantly better than the Gaussian distribution considered in [4], [14], and [15]. Indeed, as can be seen in Fig. 4, the Gamma distribution provides the best fit compared to the LogNormal and Gaussian distributions. However, when we observe the OP as shown in Fig. 4, we can see that, compared to the Gamma and LogNormal distributions, the OP associated with the Gaussian distribution shows a tangible gap between the approximate and true values at the low OP range, i.e., when the OP is less than 10^{-2}. Nevertheless, the three distributions can be used to obtain highly accurate approximate EC.

In Fig. 5, to demonstrate the impact of i.n.i.d. fading channels on the system performance, we consider different element settings, i.e., $\mathbf{L}_2$, $\mathbf{L}_3$, and $\mathbf{L}_4$. As can be observed in Fig. 5, the number of passive elements installed at the RISs

TABLE I
SIMULATION PARAMETERS

Parameters	Values	Parameters	Values
$S \rightarrow D$ distance, d_{SD} [m]	100	Avg. height of RISs' location, H [m]	10
Number of RISs, N	5	Total reflecting elements, $\sum_n L_n$	$[125, 200]$
Amplitude reflection coef., κ_{nl}	1 [25]	Bandwidth, BW [MHz]	10 [25]
Carrier frequency, f_c [GHz]	3 [25]	Nakagami shape parameter, m	$\sim \mathcal{U}[2, 3]$
CDP at RIS, $\tilde{P}_{nl}$ [mW]	7.8 [26]	Target SE, R_{th} [b/s/Hz]	1
CDP at S, $\tilde{P}_{\text{S}}$, and D, $\tilde{P}_{\text{D}}$ [mW]	10 [26]	Thermal noise power density [dBm/Hz]	-174 [25]
Transmit power, P_{S} [dBm]	$[0, 30]$	RIS's coordinate [m]	$x_{\text{R}_n} \sim \mathcal{U}[5, 95]$, $y_{\text{R}_n} \sim \mathcal{U}[1, 9]$
Antenna gain G_{S}, G_{D}, G_{R_n} [dB]	5 [25]	Noise figure, NF [dBm]	10 [25]

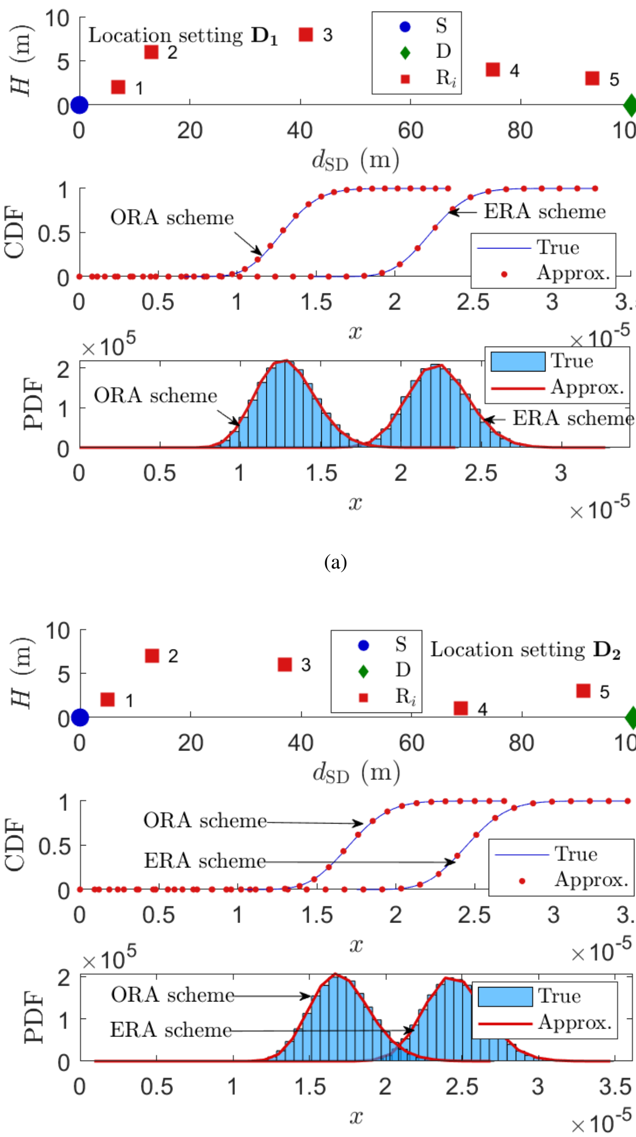

(a)

(b)

Fig. 2. Graphical demonstration of the estimated true distributions and the obtained approximated distributions in (a) Theorems 1 and 3 and (b) Theorems 2 and 4.

has a significant impact on both the OP and EC. It is because under i.n.i.d. fading channels, each RIS is subject to different fading severity, i.e., the Nakagami-m distributions between different RISs have different shape parameters and spread parameters. When comparing the performance gaps between different element settings, the ORA scheme is more sensitive than the ERA scheme to the changes of element settings. For instance, as shown in Fig. 5a, when changing from element setting $\mathbf{L}_4$ to $\mathbf{L}_2$, the transmit power of the ERA scheme needs to compensate 1.8 dBm whereas the ORA scheme needs to compensate 6.3 dBm to achieve the same OP of 10^{-4}. In addition, it is evidenced from Fig. 5 that RIS-aided systems are superior to non-RIS-aided systems, and that the ERA scheme outperforms the ORA scheme. The reason behind this is that the more of the reflecting elements that are installed, the better the performance that can be achieved.

In Fig. 6, taking into account the circuit dissipation power (CDP) in the transceivers and the RIS hardware, we evaluate the EE of the ERA and the ORA schemes. The total power consumed, P_{tol}, by a RIS-aided system can be expressed as [26]

$$P_{\text{tol}} = P_{\text{S}} + \sum_{n=1}^{N} \sum_{l=1}^{L_n} \tilde{P}_{nl} + \tilde{P}_{\text{S}} + \tilde{P}_{\text{D}},$$

where $\tilde{P}_{nl}$, $\tilde{P}_{\text{S}}$, $\tilde{P}_{\text{D}}$ are the CDP at the l-th element of the n-th RIS, S, and D, respectively. The EE of a RIS-aided system can be defined as $\text{EE} = \text{BW} \times R_{\text{th}}/P_{\text{tol}}$ [Mbit/Joule] [12], where BW and R_{th} denote the bandwidth and the target SE. As shown in Fig. 6, for element setting $\mathbf{L}_3$, when $R_{\text{th}} \leq \check{R} = 12$ b/s/Hz, where $\check{R}$ denotes the crossing point as illustrated in Fig. 6, the ORA scheme achieves higher EE than the ERA scheme, and vice-versa when $R_{\text{th}} \geq \check{R} = 12$ b/s/Hz. In addition, the element setting strongly impacts the EE, i.e., when the element setting is $\mathbf{L}_2$ and $\mathbf{L}_4$, the crossing points are $\check{R} = 12.5$ and 15.5 b/s/Hz, respectively.

In Fig. 7, we compare the performance of the distributed multi-RIS-aided scheme, i.e., the ERA scheme, versus a centralized RIS (C-RIS)-aided system. Specifically, in the centralized-ERA scheme, we assume that all elements are installed at one large C-RIS, and we let the C-RIS moves along a horizontal line from $S \rightarrow D$ as depicted in Fig. 7, where the unfilled red squares are the possible locations of the C-RIS. From various location and reflecting element settings, we can observe a common behavior, i.e., as the C-RIS is located near either S or D, the centralized-ERA scheme gives a larger EC than the distributed scheme. Meanwhile, when the C-RIS moves further away from either S or D, the ERA scheme provides a better EC.

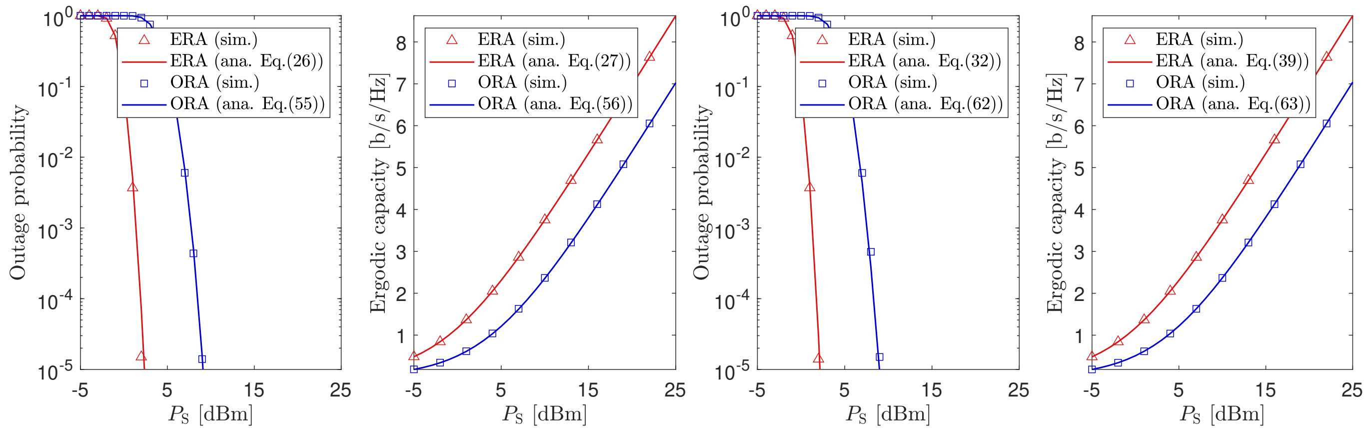

Fig. 3. OP and EC of the ERA and the ORA schemes as a function of transmit power of S, P_S [dBm].

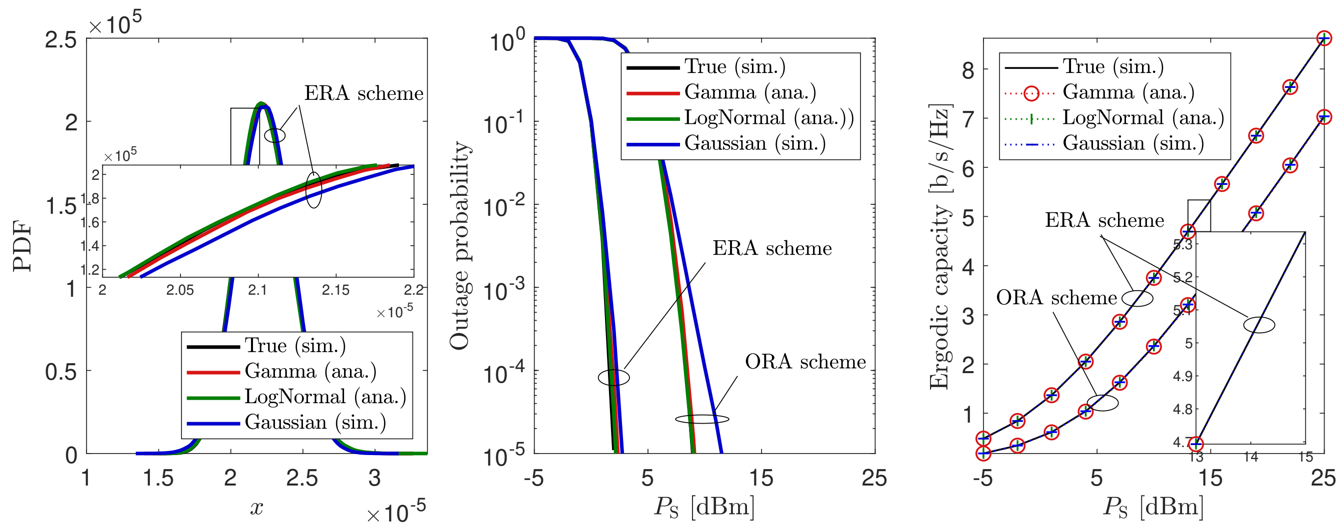

Fig. 4. Accuracy comparison of approximations between Gamma, LogNormal, and Gaussian distributions.

VI. Conclusions

In this paper, we proposed two multi-RIS-aided schemes, namely the ERA and the ORA schemes. We focused on the statistical characterization and modeling of the two schemes. Toward this end, we proposed a mathematical framework to determine the distribution of the e2e fading channel in both schemes. Specifically, for the ERA scheme, the framework determined that the true distribution of the magnitude of the e2e channel coefficient can be approximated by either the Gamma or LogNormal distributions. For the ORA scheme, we obtained approximate closed-form expressions for the CDF and PDF of the magnitude of the e2e channel. Moreover, the framework determined that the ORA scheme's fading channel can also be modeled by a LogNormal distribution. Based on the resultant fading models, we evaluated the performance of the two schemes in terms of OP and EC. Numerical results showed that the ERA scheme outperforms the ORA scheme in terms of OP and EC. Nevertheless, the ORA scheme achieves better EE than the ERA scheme for some specific values of the target SE. We showed that for a given total number of passive elements, the element allocation and RISs' position have a significant impact on the system performance. On the other hand, the centralized large-RIS-aided system can yield a better EC than the ERA scheme when the centralized RIS is located near either the source or the destination; otherwise, the ERA scheme outperforms the centralized RIS-aided system.

Appendix A
Proof of Theorem 1

Since $h_0 \sim \text{Nakagami}(m_0, \Omega_0)$, the k-th moment of h_0, $\mu_{h_0}(k) \triangleq \mathbb{E}[h_0^k]$, can be obtained as

$$\mu_{h_0}(k) = \frac{\Gamma(m_0 + k/2)}{\Gamma(m_0)} \left(\frac{m_0}{\Omega_0}\right)^{-k/2}. \tag{64}$$

We now turn our focus to the k-th moment of U_{nl}. The

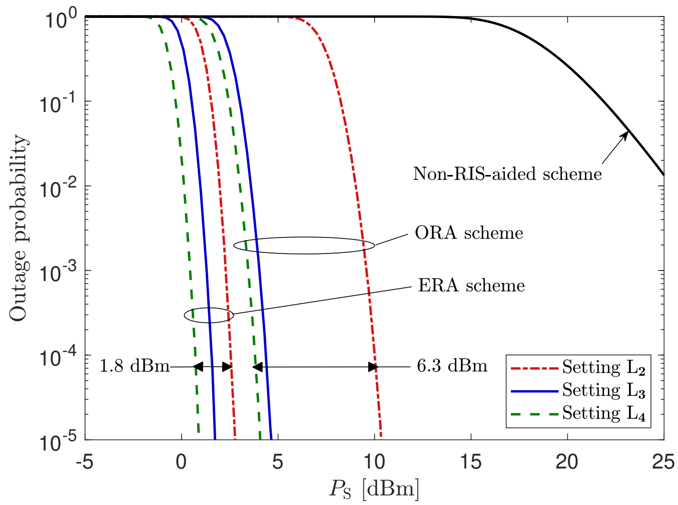

(a)

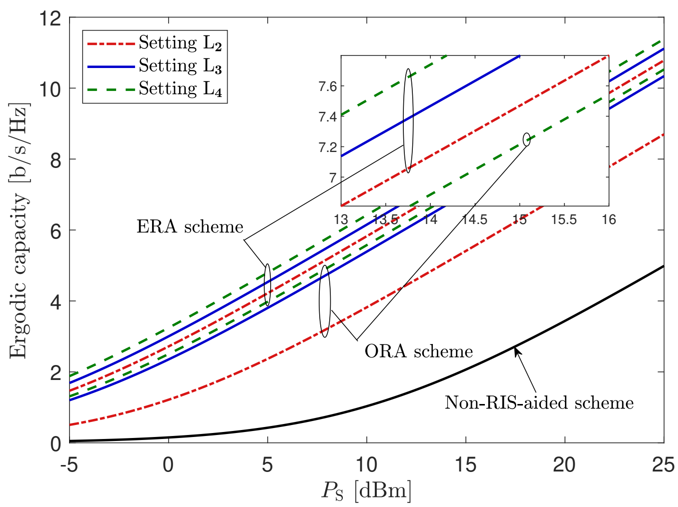

(b)

Fig. 5. Analysis of the impact of the number of reflecting elements on (a) the OP and (b) the EC of the ERA and the ORA schemes, respectively, with $R_{\text{th}} = 3$ b/s/Hz.

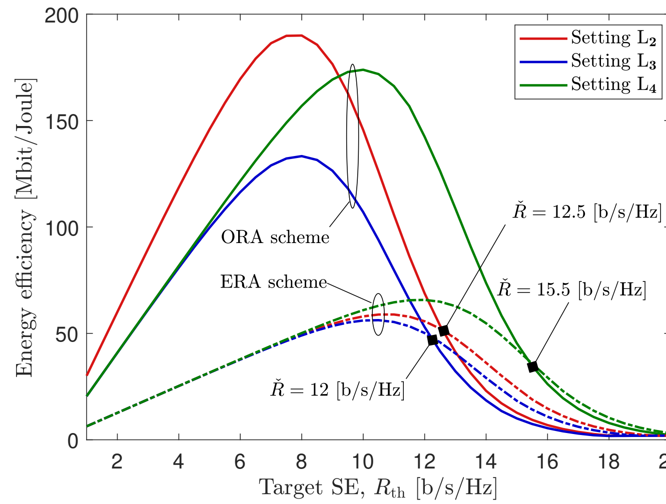

Fig. 6. Energy efficiency [Mbit/Joule] of the ERA and the ORA schemes as a function of target SE, R_{th} [b/s/Hz].

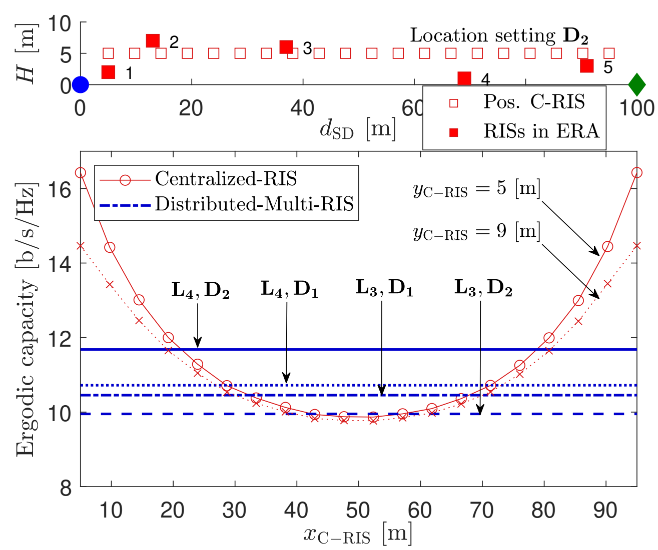

Fig. 7. Performance comparison between centralized versus distributed RIS-aided systems, with $P_S = 23$ dBm.

exact PDF of U_{nl} is obtained as

$$f_{U_{nl}}(z) = \frac{4\lambda_{nl}^{m_{\text{h}_n}+m_{\text{g}_n}}}{\Gamma(m_{\text{h}_n})\Gamma(m_{\text{g}_n})} x^{m_{\text{h}_n}+m_{\text{g}_n}-1} K_{m_{\text{g}_n}-m_{\text{h}_n}}(2\lambda_{nl}z), \quad (65)$$

where $\lambda_{nl} = \sqrt{\frac{1}{\kappa_{nl}^2}\frac{m_{\text{h}_n}}{\Omega_{\text{h}_n}}\frac{m_{\text{g}_n}}{\Omega_{\text{g}_n}}}$. The detailed derivation of (65) can be briefly presented as follows.

The aim of this derivation is not only to present the exact PDF of U_{nl} but also to point out that the magnitude of the synthesized channel of the individual dual-hop channel with respect to a single reflecting element of a RIS in our considered system follows a Generalized-K (K_G) distribution. Recall that, for a given n, $U_{nl} = \kappa_{nl}h_{nl}g_{nl}$, where $U_{n1}, ..., U_{nL_n}$ are i.i.d. RVs, but h_{nl} and g_{nl} are i.n.i.d. RVs, $\forall n, \forall l$. Specifically, knowing that $f_{XY}(z) = \int_0^\infty \frac{1}{x} f_Y\left(\frac{z}{x}\right) f_X(x)dx$, the PDF of U_{nl} can be written as

$$f_{U_{nl}}(z) = \frac{1}{\kappa_{nl}}\int_0^\infty \frac{1}{x} f_{h_{nl}}\left(\frac{z}{\kappa_{nl}x}\right) f_{g_{nl}}(x)dx. \quad (66)$$

Recall that $h_{nl} \sim \text{Nakagami}(m_{\text{h}_n}, \Omega_{\text{h}_n})$ and $g_{nl} \sim \text{Nakagami}(m_{\text{g}_n}, \Omega_{\text{g}_n})$, from (10), we have

$$f_{U_{nl}}(z) = \frac{4}{\Gamma(m_{\text{h}_n})\Gamma(m_{\text{g}_n})}\left(\frac{1}{\kappa_{nl}^2}\frac{m_{\text{h}_n}}{\Omega_{\text{h}_n}}\right)^{m_{\text{h}_n}}\left(\frac{m_{\text{g}_n}}{\Omega_{\text{g}_n}}\right)^{m_{\text{g}_n}} z^{2m_{\text{h}_n}-1} \times \int_0^\infty x^{2m_{\text{g}_n}-2m_{\text{h}_n}-1} e^{\left(-\frac{z^2}{\kappa_{nl}^2}\frac{m_{\text{h}_n}}{\Omega_{\text{h}_n}}\frac{1}{x^2} - \frac{m_{\text{g}_n}}{\Omega_{\text{g}_n}}x^2\right)} dx. \quad (67)$$

Making use of [21, Eq. (3.478.4)], the exact PDF of U_{nl} is obtained as in (65). Thus, we can conclude that U_{nl} follows a K_G distribution with the shaping parameters m_{g_n} and m_{h_n}. Based on the exact PDF of U_{nl}, we are going to derive the k-th moment of U_{nl}, which is defined as $\mu_{U_{nl}}(k) \triangleq \mathbb{E}[U_{nl}^k] = \int_0^\infty z^k f_{U_{nl}}(z)dz$. From (65) and after some mathematical manipulations, $\mu_{U_{nl}}(k)$ can be obtained as

$$\mu_{U_{nl}}(k)=\lambda_{nl}^{-k}\frac{\Gamma(m_{\mathrm{h}_n}+k/2)\Gamma(m_{\mathrm{g}_n}+k/2)}{\Gamma(m_{\mathrm{h}_n})\Gamma(m_{\mathrm{g}_n})}. \tag{68}$$

The exact PDF of U_{nl} in (65) helps derive the k-th moment of U_{nl}, however, it makes the derivation of closed-form expressions for the CDF and PDF of Z intractable. To circumvent this problem, based on the obtained k-th moment of U_{nl} in (68), we fit U_{nl} to a Gamma distribution. Note that for a given n, the U_{nl} RVs are i.i.d. with respect to $l=1,...,L_n$. Relying on Step 2 in our framework, we have

$$U_{nl} \overset{\text{approx.}}{\sim} \mathrm{Gamma}(\alpha_{U_n},\beta_{U_n}), \tag{69}$$

where

$$\alpha_{U_n}=\frac{(\mathbb{E}[U_{nl}])^2}{\mathrm{Var}[U_{nl}]}=\frac{[\mu_{U_{nl}}(1)]^2}{\mu_{U_{nl}}(2)-[\mu_{U_{nl}}(1)]^2}, \tag{70}$$

$$\beta_{U_n}=\frac{\mathbb{E}[U_{nl}]}{\mathrm{Var}[U_{nl}]}=\frac{\mu_{U_{nl}}(1)}{\mu_{U_{nl}}(2)-[\mu_{U_{nl}}(1)]^2}, \tag{71}$$

and $f_{U_{nl}}(z;\alpha_{U_n},\beta_{U_n})$ is expressed as in (12). The analysis will rely on the approximate PDF of U_{nl}. In addition, for a given n-th RIS, we consider fixed amplitude reflection coefficients [25], i.e., $\kappa_{nl}=\kappa_n, \forall l$.

The approximate distribution of V_n can be obtained as

$$V_n \overset{\text{approx.}}{\sim} \mathrm{Gamma}(L_n\alpha_{U_n},\beta_{U_n}) \tag{72}$$

Consequently, the approximate CDF and PDF of V_n are obtained as

$$F_{V_n}(z)\approx\frac{\gamma(L_n\alpha_{U_n},\beta_{U_n}z)}{\Gamma\left(L_n\alpha_{U_n}\right)}, \tag{73}$$

$$f_{V_n}(z)\approx f_{V_n}(z;L_n\alpha_{U_n},\beta_{U_n}), \tag{74}$$

where $f_{V_n}(z;L_n\alpha_{U_n},\beta_{U_n})$ is expressed as in (12). Making use of a multinomial expansion [36], the k-th moment of V_n, i.e., $\mu_{V_n}(k)\triangleq\mathbb{E}[V_n^k]$, can be obtained as

$$\begin{aligned}\mu_{V_n}(k)=&\sum_{k_1=0}^{k}\sum_{k_2=0}^{k_1}\cdots\sum_{k_{L_n-1}=0}^{k_{L_n-2}}\binom{k}{k_1}\binom{k_1}{k_2}\cdots\binom{k_{L_n-2}}{k_{L_n-1}}\\&\times\mu_{U_{n1}}(k-k_1)\mu_{U_{n2}}(k_1-k_2)...\mu_{U_{nL_n}}(k_{L_n-1}).\end{aligned} \tag{75}$$

We turn our focus to the k-th moment of T, i.e., $\mu_T(k)\triangleq\mathbb{E}[T^k]$. Proceeding in a similar manner, the k-th moment of T, i.e., $\mu_T(k)\triangleq\mathbb{E}[T^k]$, can be obtained as

$$\begin{aligned}\mu_T(k)=&\sum_{k_1=0}^{k}\sum_{k_2=0}^{k_1}\cdots\sum_{k_{N-1}=0}^{k_{N-2}}\binom{k}{k_1}\binom{k_1}{k_2}\cdots\binom{k_{N-2}}{k_{N-1}}\\&\times\mu_{V_1}(k-k_1)\mu_{V_2}(k_1-k_2)...\mu_{V_n}(k_{N-1}).\end{aligned} \tag{76}$$

From (68), (75), and (76), the first and second moments of T can be expressed as

$$\mu_T(1)=\sum_{n=1}^{N}\sum_{l=1}^{L_n}\mu_{U_{nl}}(1), \tag{77}$$

$$\begin{aligned}\mu_T(2)=&\sum_{n=1}^{N}\left[\sum_{l=1}^{L_n}\mu_{U_{nl}}(2)+2\sum_{l=1}^{L_n}\mu_{U_{nl}}(1)\sum_{l'=l+1}^{L_n}\mu_{U_{nl'}}(1)\right]\\&+2\sum_{n=1}^{N}\left[\sum_{l=1}^{L_n}\mu_{U_{nl}}(1)\right]\sum_{n'=n+1}^{N}\left[\sum_{l=1}^{L_{n'}}\mu_{U_{n'l}}(1)\right].\end{aligned} \tag{78}$$

Since h_0 and T are independent, the k-th moment of Z, $\mu_Z(k)\triangleq\mathbb{E}[Z^k]$, can be obtained via the moments of its summands, i.e., h_0 and T, by applying the binomial theorem. Thus, $\mu_Z(k)$ can be obtained as

$$\begin{aligned}\mu_Z(k)&=\mathbb{E}[(h_0+T)^k]\\&=\mathbb{E}\left[\sum_{l=0}^{k}\binom{k}{l}h_0^lT^{l-k}\right]\\&=\sum_{l=0}^{k}\binom{k}{l}\mu_{h_0}(l)\mu_T(l-k).\end{aligned} \tag{79}$$

Thus, from (79), we have

$$\mu_Z(1)=\mu_{h_0}(1)+\mu_T(1), \tag{80}$$

$$\mu_Z(2)=\mu_{h_0}(2)+\mu_T(2)+2\mu_{h_0}(1)\mu_T(1). \tag{81}$$

From (64), we have

$$\mu_{h_0}(1)=\frac{\Gamma(m_0+1/2)}{\Gamma(m_0)}\left(\frac{m_0}{\Omega_0}\right)^{-1/2}, \tag{82}$$

$$\mu_{h_0}(2)=\frac{\Gamma(m_0+1)}{\Gamma(m_0)}\frac{\Omega_0}{m_0}=\Omega_0. \tag{83}$$

Plugging (82) and (77) into (80), and plugging (83) and (78) into (81), we complete the proof of Theorem 1.

Appendix B
Derivation of (27)

From (27), the EC of the ERA scheme can be rewritten as

$$\begin{aligned}\bar{C}^{\mathrm{ERA}}&=\int_0^\infty\log_2\left(1+z\right)f_{\bar{\rho}Z^2}(z)dz\\&=\frac{1}{\ln 2}\int_0^\infty\frac{1}{z+1}\left[1-F_Z\left(\sqrt{\frac{z}{\bar{\rho}}}\right)\right]dz.\end{aligned} \tag{84}$$

Making use of the identity [23, Eq. (8.4.2.5)], i.e., $(1+x)^{-\xi}=\frac{1}{\Gamma(\xi)}G_{1,1}^{1,1}\left(x\middle|\begin{matrix}1-\xi\\0\end{matrix}\right)$, (84) can be further expressed as

$$\bar{C}^{\mathrm{ERA}}\approx\frac{1}{\ln 2}\int_0^\infty G_{1,1}^{1,1}\left(z\middle|\begin{matrix}0\\0\end{matrix}\right)\frac{\gamma\left(\alpha_Z,\beta_Z\sqrt{\frac{z}{\bar{\rho}}}\right)}{\Gamma(\alpha_Z)}dz. \tag{85}$$

Based on [21, Eq. (8.356.3)], i.e., $\Gamma(\alpha,x)+\gamma(\alpha,x)=\Gamma(\alpha)$, we have

$$F_Z(z)=\frac{\gamma\left(\alpha_Z,\beta_Z\sqrt{\frac{z}{\bar{\rho}}}\right)}{\Gamma(\alpha_Z)}=1-\frac{\Gamma\left(\alpha_Z,\beta_Z\sqrt{\frac{z}{\bar{\rho}}}\right)}{\Gamma(\alpha_Z)}. \tag{86}$$

Using the equivalence between the incomplete Gamma function and the Meijer-G function [23, Eq. (8.4.16.2)], i.e., $\Gamma\left(\alpha_Z, \beta_Z\sqrt{\frac{z}{\bar{\rho}}}\right) = G_{1,2}^{2,0}\left(\beta_Z\sqrt{\frac{z}{\bar{\rho}}}\middle|\begin{matrix}1\\ \alpha_Z, 0\end{matrix}\right)$, (85) can be further expressed as

$$\bar{C}^{\mathrm{ERA}} \approx \frac{1}{\Gamma(\alpha_Z)\ln 2}\int_0^\infty G_{1,1}^{1,1}\left(z\middle|\begin{matrix}0\\0\end{matrix}\right) G_{1,2}^{2,0}\left(\beta_Z\sqrt{\frac{z}{\bar{\rho}}}\middle|\begin{matrix}1\\ \alpha_Z, 0\end{matrix}\right). \tag{87}$$

Next, we rely on the identity [23, Eq. (2.24.1.1)] for the general integral of

$$\int_0^\infty x^{\alpha-1} G_{u,v}^{s,t}\left(\xi x\middle|\begin{matrix}(c_u)\\(d_v)\end{matrix}\right) G_{p,q}^{m,n}\left(\omega x^{l/k}\middle|\begin{matrix}(a_p)\\(b_q)\end{matrix}\right) dx.$$

Thus, the EC of the ERA scheme can be obtained as

$$\bar{C}^{\mathrm{ERA}} \approx \frac{1}{\Gamma(\alpha_Z)\ln 2}\frac{2^{\alpha_Z-1}}{\sqrt{\pi}} G_{3,5}^{5,1}\left(\frac{(\beta_Z)^2}{4\bar{\rho}}\middle|\begin{matrix}0, \frac{1}{2}, 1\\ \frac{\alpha_Z}{2}, \frac{\alpha_Z+1}{2}, 0, \frac{1}{2}, 0\end{matrix}\right). \tag{88}$$

Appendix C
Proof of Lemma 2

The k-moment of M_V, $\mu_{M_V}(k) \triangleq \mathbb{E}[M_V^k]$, can be expressed as

$$\mu_{M_V}(k) = \sum_{n=1}^N \int_0^\infty x^k f_{V_n}(x) \prod_{\substack{t=1\\t\neq n}}^N F_{V_t}(x) dx. \tag{89}$$

Thus, we have

$$\mu_{M_V}(k) \approx \sum_{n=1}^N \int_0^\infty x^k f_{V_n}(x) \prod_{\substack{t=1\\t\neq n}}^N \frac{\gamma(L_t\alpha_{U\,t}, \beta_{U\,t})}{\Gamma(L_t\alpha_{U\,t})} dx. \tag{90}$$

The $\gamma(\cdot,\cdot)$ in (73) can be re-expressed as [37, Eq. (6.5.29)]

$$\frac{\gamma(L_t\alpha_{U_n}, \beta_{U\,t}x)}{\Gamma(L_t\alpha_{U\,t})} = e^{-\beta_{U\,t}x}\sum_{w_t=0}^\infty \frac{(\beta_{U\,t}x)^{L_t\alpha_{U\,t}+w_t}}{\Gamma(L_t\alpha_{U\,t}+w_t+1)}. \tag{91}$$

Plugging (91) into $\prod_{\substack{t=1\\t\neq n}}^N F_{V_t}(x)$, after some mathematical manipulations, we have

$$\prod_{\substack{t=1\\t\neq n}}^N \frac{\gamma(L_t\alpha_{U\,t}, \beta_{U\,t})}{\Gamma(L_t\alpha_{U\,t})} = e^{-x\sum_{\substack{t=1\\t\neq n}}^N \beta_{U\,t}} \widetilde{\sum_{\substack{w_t\\t\neq n}}}\left[\prod_{\substack{t=1\\t\neq n}}^N \frac{(\beta_{U\,t}x)^{L_t\alpha_{U\,t}+w_t}}{\Gamma(L_t\alpha_{U\,t}+w_t+1)}\right], \tag{92}$$

where

$$\widetilde{\sum_{\substack{w_t\\t\neq n}}} \triangleq \sum_{w_1=0}^\infty \ldots \sum_{w_{n-1}=0}^\infty \sum_{w_{n+1}=0}^\infty \ldots \sum_{w_N=0}^\infty .$$

Thus, we have

$$\mu_{M_V}(k) \approx \sum_{n=1}^N \widetilde{\sum_{\substack{w_t\\t\neq n}}}\left[\prod_{\substack{t=1\\t\neq n}}^N \frac{(\beta_{U\,t}x)^{L_t\alpha_{U\,t}+w_t}}{\Gamma(L_t\alpha_{U\,t}+w_t+1)}\right] \times \int_0^\infty \frac{(\beta_{U_n})^{L_n\alpha_{U_n}}}{\Gamma(L_n\alpha_{U_n})} x^{\sum_{j=1}^N L_j\alpha_{U\,j} + \sum_{\substack{t=1\\t\neq n}} w_t + k - 1} \times e^{-x\sum_{i=1}^N \beta_{U\,i}} dx. \tag{93}$$

Let us denote $\Psi_{\tilde{n}} \triangleq \sum_{\substack{t=1\\t\neq n}}^N w_t$ and $\Lambda \triangleq \sum_{t=1}^N L_t\alpha_{U\,t}$. After some mathematical manipulations, $\mu_{M_V}(k)$ can be expressed as

$$\mu_{M_V}(k) \approx \sum_{n=1}^N \widetilde{\sum_{\substack{w_t\\t\neq n}}}\left[\prod_{\substack{t=1\\t\neq n}}^N \frac{(\beta_{U\,t}x)^{L_t\alpha_{U\,t}+w_t}}{\Gamma(L_t\alpha_{U\,t}+w_t+1)}\right] \frac{(\beta_{U_n})^{L_n\alpha_{U_n}}}{\Gamma(L_n\alpha_{U_n})} \times \int_0^\infty x^{\Lambda+\Psi_{\tilde{n}}+k-1} e^{-x\sum_{i=1}^N \beta_{U\,i}} dx. \tag{94}$$

Making use of the identity $\int_0^\infty x^{v-1}e^{-px} = \Gamma(v)/p^v$ [21, Eq. (3.381.4)], the integral in (94) can be derived as

$$\mu_{M_V}(k) \approx \sum_{n=1}^N \left\{ \widetilde{\sum_{\substack{w_t\\t\neq n}}}\left[\prod_{\substack{t=1\\t\neq n}}^N \frac{(\beta_{U\,t}x)^{L_t\alpha_{U\,t}+w_t}}{\Gamma(L_t\alpha_{U\,t}+w_t+1)}\right] \times \frac{(\beta_{U_n})^{L_n\alpha_{U_n}}}{\Gamma(L_n\alpha_{U_n})}\Gamma(\Lambda+\Psi_{\tilde{n}}+k) \times \left[\sum_{i=1}^N \beta_{U\,i}\right]^{-(\Lambda+\Psi_{\tilde{n}}+k)} \right\}. \tag{95}$$

After some rearrangements, we obtain μ_{M_V} as in (96).

Let $\chi_t = \beta_{U\,t}/\sum_{t=1}^N \beta_{U\,t}$. It can be observed that $\chi_t \in (0,1)$ and $\sum_{t=1}^N \chi_t = 1$, which yields

$$\left[(\beta_{U_n})^{L_n\alpha_{U_n}} \prod_{\substack{t=1\\t\neq n}}^N {\beta_{U\,t}}^{L_t\alpha_{U\,t}}\right]\left[\sum_{i=1}^N \beta_{U\,i}\right]^{(-\Lambda)} = \prod_{j=1}^N (\chi_j)^{L_j\alpha_{U\,j}}, \tag{97}$$

By plugging (97) into (96), we obtain μ_{M_V} as in (98). After some mathematical manipulations, it follows that

$$\left[\prod_{\substack{t=1\\t\neq n}}^N \frac{(\beta_{U\,t})^{w_t}}{\Gamma(L_t\alpha_{U\,t}+w_t+1)}\right]\left[\sum_{i=1}^N \beta_{U\,i}\right]^{-\Psi_{\tilde{n}}} = \prod_{\substack{t=1\\t\neq n}} \frac{1}{\Gamma(L_t\alpha_{U\,t}+w_t+1)} \prod_{\substack{t=1\\t\neq n}} (\chi_t)^{-\Psi_{\tilde{n}}}. \tag{99}$$

Note that, in (99), i is independent from t. Next, let $\langle x\rangle_n \triangleq \Gamma(x+n)/\Gamma(x)$ denote a *Pochhammer symbol*, which implies

$$\Gamma(\Lambda+k+\Psi_{\tilde{n}}) = \langle \Lambda+k\rangle_{\Psi_{\tilde{n}}}\Gamma(\Lambda+k). \tag{100}$$

Thus, the RHS of (99) can be expressed as

$$\prod_{\substack{t=1\\t\neq n}} \frac{(\chi_t)^{-\Psi_{\tilde{n}}}}{\Gamma(L_t\alpha_{U\,t}+w_t+1)} = \left[\prod_{\substack{t=1\\t\neq n}} \frac{1}{\Gamma(L_t\alpha_{U\,t}+1)}\right]\left[\prod_{\substack{t=1\\t\neq n}} \frac{\langle 1\rangle_{w_t}}{\langle L_t\alpha_{U\,t}+1\rangle_{w_t}}\right]\left[\prod_{\substack{t=1\\t\neq n}}^N \frac{(\chi_t)^{w_t}}{w_t!}\right]. \tag{101}$$

$$\mu_{M_V}(k) \approx \sum_{n=1}^{N} \Bigg\{ \frac{1}{\Gamma(L_n \alpha_{U t})} \Bigg[(\beta_{U_n})^{L_n \alpha_{U_n}} \prod_{\substack{t=1 \\ t \neq n}}^{N} (\beta_{U t})^{L_t \alpha_{U t}} \Bigg] \Bigg[\sum_{t=i}^{N} \beta_{U i} \Bigg]^{-(\Lambda+k)} \times \widetilde{\sum_{\substack{w_t \\ t\neq n}}} \Gamma(\Lambda + \Psi_{\check{n}} + k) \Bigg[\prod_{\substack{t=1 \\ t \neq n}}^{N} \frac{(\beta_{U t})^{w_t}}{\Gamma(L_t \alpha_{U t} + w_t + 1)} \Bigg] \Bigg[\sum_{i=1}^{N} \beta_{U i} \Bigg]^{-\Psi_{\check{n}}} \Bigg\}. \tag{96}$$

$$\mu_{M_V}(k) \approx \sum_{n=1}^{N} \Bigg\{ \frac{1}{\Gamma(L_n \alpha_{U t})} \Bigg[\prod_{j=1}^{N} (\chi_j)^{L_j \alpha_{U j}} \Bigg] \Bigg[\sum_{i=1}^{N} \beta_{U i} \Bigg]^{-k} \times \widetilde{\sum_{\substack{w_t \\ t\neq n}}} \Gamma(\Lambda + \Psi_{\check{n}} + k) \Bigg[\prod_{\substack{t=1 \\ t \neq n}}^{N} \frac{(\beta_{U t})^{w_t}}{\Gamma(L_t \alpha_{U t} + w_t + 1)} \Bigg] \Bigg[\sum_{i=1}^{N} \beta_{U i} \Bigg]^{-\Psi_{\check{n}}} \Bigg\}. \tag{98}$$

After some mathematical manipulations, we have

$$\mu_{M_V}(k) \approx \Bigg[\sum_{i=1}^{N} \beta_{U i} \Bigg]^{-k} \Bigg[\prod_{j=1}^{N} (\chi_j)^{L_j \alpha_{U j}} \Bigg] \times \sum_{n=1}^{N} \Bigg\{ \frac{\Gamma(\Lambda + k)}{\Gamma(L_n \alpha_{U_n})} \Bigg[\prod_{\substack{t=1 \\ t \neq n}}^{N} \frac{1}{\Gamma(L_n \alpha_{U_n} + 1)} \Bigg] \times \widetilde{\sum_{\substack{w_t \\ t\neq n}}} \Bigg[\frac{\langle \Lambda + k \rangle_{\sum_{\substack{t=1 \\ t\neq n}}^{N} w_t} \prod_{\substack{t=1 \\ t\neq n}}^{N} \langle 1 \rangle_{w_t}}{\prod_{\substack{t=1 \\ t\neq n}}^{N} \langle L_t \alpha_{U t} + 1 \rangle_{w_t}} \prod_{\substack{t=1 \\ t \neq n}}^{N} \frac{(\chi_t)^{w_t}}{w_t!} \Bigg] \Bigg\}. \tag{102}$$

Using the series representation of the Lauricell function Type-A [24, Eq.(1.4.1)], and relying on its integral representation [24, Eq.(9.4.35)], we obtain the approximated closed-form expression for $\mu_{M_V}(k)$ in (61). This completes the proof of Lemma 2.

REFERENCES

[1] M. Di Renzo, A. Zappone, M. Debbah, M.-S. Alouini, C. Yuen, J. de Rosny, and S. Tretyakov, "Smart radio environments empowered by reconfigurable intelligent surfaces: How it works, state of research, and the road ahead," *IEEE J. Sel. Areas Commun.*, vol. 38, no. 11, pp. 2450–2525, Nov. 2020.

[2] Q. Wu and R. Zhang, "Intelligent reflecting surface enhanced wireless network via joint active and passive beamforming," *IEEE Trans. Wireless Commun.*, vol. 18, no. 11, pp. 5394–5409, Nov. 2019.

[3] C. Liaskos, S. Nie, A. Tsioliaridou, A. Pitsillides, S. Ioannidis, and I. Akyildiz, "End-to-end wireless path deployment with intelligent surfaces using interpretable neural networks," *IEEE Trans. Commun.*, vol. 68, no. 11, pp. 6792–6806, Nov. 2020.

[4] D. L. Galappaththige, D. Kudathanthirige, and G. A. A. Baduge, "Performance analysis of distributed intelligent reflective surfaces for wireless communications," Oct. 2020. [Online]. Available: http://arxiv.org/abs/2010.12543

[5] B. Tahir, S. Schwarz, and M. Rupp, "Analysis of uplink IRS-assisted NOMA under Nakagami-m fading via moments matching," *IEEE Wireless Commun. Lett.*, 2020, DOI: 10.1109/LWC.2020.3043810.

[6] E. Basar, M. Di Renzo, J. De Rosny, M. Debbah, M.-S. Alouini, and R. Zhang, "Wireless communications through reconfigurable intelligent surfaces," *IEEE Access*, vol. 7, pp. 116 753–116 773, Jun. 2019.

[7] F. A. P. de Figueiredo, M. S. P. Facina, R. C. Ferreira, Y. Ai, R. Ruby, Q.-V. Pham, and G. Fraidenraich, "Large intelligent surfaces with discrete set of phase-shifts communicating through double-rayleigh fading channels," *IEEE Access*, vol. 9, pp. 20 768–20 787, Feb. 2021.

[8] M.-A. Badiu and J. P. Coon, "Communication through a large reflecting surface with phase errors," *IEEE Wireless Commun. Lett.*, vol. 9, no. 2, pp. 184–188, Feb. 2020.

[9] A.-A. A. Boulogeorgos and A. Alexiou, "Performance analysis of reconfigurable intelligent surface-assisted wireless systems and comparison with relaying," *IEEE Access*, vol. 8, pp. 94 463–94 483, Jun. 2020.

[10] M. H. Samuh and A. M. Salhab, "Performance analysis of reconfigurable intelligent surfaces over Nakagami-m fading channels," pp. 15–18, Oct. 2020. [Online]. Available: http://arxiv.org/abs/2010.07841

[11] X. Gan, C. Zhong, Y. Zhu, and Z. Zhong, "User selection in reconfigurable intelligent surface assisted communication systems," *IEEE Commun. Lett.*, 2021, DOI: 10.1109/LCOMM.2020.3048782.

[12] E. Bjornson and L. Sanguinetti, "Rayleigh fading modeling and channel hardening for reconfigurable intelligent surfaces," *IEEE Wireless Commun. Lett.*, 2020, DOI: 10.1109/LWC.2020.3046107.

[13] T. Van Chien, A. K. Papazafeiropoulos, L. T. Tu, R. Chopra, S. Chatzinotas, and B. Ottersten, "Outage probability analysis of IRS-assisted systems under spatially correlated channels," 2021. [Online]. Available: http://arxiv.org/abs/2102.11408

[14] M. Jung, W. Saad, Y. Jang, G. Kong, and S. Choi, "Performance analysis of large intelligent surfaces (LISs): Asymptotic data rate and channel hardening effects," *IEEE Trans. Wireless Commun.*, vol. 19, no. 3, pp. 2052–2065, Mar. 2020.

[15] L. Yang, Y. Yang, D. B. da Costa, and I. Trigui, "Outage probability and capacity scaling law of multiple RIS-aided networks," *IEEE Wireless Commun. Lett.*, vol. 10, no. 2, pp. 256–260, Feb. 2021.

[16] Y. Fang, S. Atapattu, H. Inaltekin, and J. Evans, "Optimum reconfigurable intelligent surface selection for indoor and outdoor communications," Dec. 2020. [Online]. Available: http://arxiv.org/abs/2012.11793

[17] W. Mei and R. Zhang, "Cooperative beam routing for multi-IRS aided communication," *IEEE Wireless Commun. Lett.*, vol. 10, no. 2, pp. 426–430, Feb. 2021.

[18] S. Zhang and R. Zhang, "Intelligent reflecting surface aided multiple access: Capacity region and deployment strategy," Feb. 2020. [Online]. Available: http://arxiv.org/abs/2002.07091

[19] I. Yildirim, A. Uyrus, and E. Basar, "Modeling and analysis of reconfigurable intelligent surfaces for indoor and outdoor applications in future wireless networks," *IEEE Trans. Commun.*, 2020, DOI: 10.1109/TCOMM.2020.3035391.

[20] T. N. Do, G. Kaddoum, T.-L. Nguyen, D. B. da Costa, and Z. J. Haas, "Simulation code," Feb. 2021. [Online]. Available: https://github.com/trinhudo/Multi-RIS

[21] I. S. Gradshteyn and I. M. Ryzhik, *Tables of Integrals, Series, and Products*, 7th ed. New York, NY, USA: Academic Press, 2007.

[22] M. Abramowitz and I. A. Stegun, *Handbook of Mathematical Functions: With Formulas, Graphs, and Mathematical Tables*. New York, NY, USA: Dover, 1965.

[23] A. Prudnikov, Y. Brychkov, and O. Marichev, *Integrals and Series, Volume 3: More Special Functions*. Boca Raton, FL, USA: CRC Press, 1999.

[24] H. M. Srivastava and P. W. Karlsson, *Multiple Gaussian Hypergeometric Series*. Hoboken, NJ, USA: Wiley, 1985.

[25] E. Bjornson, O. Ozdogan, and E. G. Larsson, “Intelligent reflecting surface versus decode-and-forward: How large surfaces are needed to beat relaying?” *IEEE Wireless Commun. Lett.*, vol. 9, no. 2, pp. 244–248, Feb. 2020.

[26] C. Huang, A. Zappone, G. C. Alexandropoulos, M. Debbah, and C. Yuen, “Reconfigurable intelligent surfaces for energy efficiency in wireless communication,” *IEEE Trans. Wirel. Commun.*, vol. 18, no. 8, pp. 4157–4170, Aug. 2019.

[27] L. Yang, F. Meng, J. Zhang, M. O. Hasna, and M. D. Renzo, “On the performance of RIS-assisted dual-hop UAV communication systems,” *IEEE Transactions on Vehicular Technology*, vol. 69, no. 9, pp. 10 385–10 390, Sep. 2020.

[28] *MATLAB version R2021a*, The Mathworks, Inc., Natick, MA, USA, 2021.

[29] K. O. Bowman and L. R. Shenton, *Estimator: Method of Moments*. Hoboken, NJ, USA: Wiley, 1998.

[30] P. Z. Peebles, *Probability, Random Variables and Random Signal Principles*, 4th ed. New York, NY, USA: McGraw-Hill Science, 2000.

[31] P. S. Bithas, V. Nikolaidis, A. G. Kanatas, and G. K. Karagiannidis, “UAV-to-ground communications: Channel modeling and UAV selection,” *IEEE Trans. Commun.*, vol. 68, no. 8, pp. 5135–5144, Aug. 2020.

[32] E. W. Stacy, “A generalization of the gamma distribution,” *The Annals of Mathematical Statistics*, vol. 33, no. 3, pp. 1187–1192, Sep. 1962.

[33] L. Fenton, “The sum of log-normal probability distributions in scatter transmission systems,” *IEEE Trans. Commun.*, vol. 8, no. 1, pp. 57–67, 1960.

[34] A. Laourine, A. Stéphenne, and S. Affes, “Estimating the ergodic capacity of Log-Normal channels,” *IEEE Commun. Lett.*, vol. 11, no. 7, pp. 568–570, Jul. 2007.

[35] “Evolved universal terrestrial radio access (E-UTRA); further advancements for e-utra physical layer aspects (release 9),” *Document 3GPP-TR-36.814 V9.0.0*, Mar. 2010.

[36] D. B. da Costa, H. Ding, and J. Ge, “Interference-limited relaying transmissions in dual-pop cooperative networks over Nakagami-m fading,” *IEEE Commun. Lett.*, vol. 15, no. 5, pp. 503–505, May 2011.

[37] M. Abramowitz and I. A. Stegun, *Handbook of Mathematical Functions with Formulas, Graphs, and Mathematical Tables*. New York, NY, USA: Dover Books, 1972.